PROSJEKTRAPPORT

ISSN 0071-5638

HAVFORSKNINGSINSTITUTTET
MILJØ - RESSURS - HAVBRUK

Nordnesgt. 50 Postboks 1870 5024 Bergen
Tlf.: 55 23 85 00 Faks: 55 23 85 31

Forskningsstasjonen	Austevoll	Matre
Flødevigen	Havbruksstasjon	Havbruksstasjon
4817 His	5392 Storebø	5198 Matredal
Tlf.: 37 05 90 00	Tlf.: 56 18 03 42	Tlf.: 56 36 60 40
Faks: 37 05 90 01	Faks: 56 18 03 98	Faks: 56 36 61 43

Distribusjon:
ÅPEN

HI-prosjektnr.:
0408.1

Oppdragsgiver(e):
Det Kgl. Nærings- og Energidepartementet

Oppdragsgivers referanse:
AKUP-prosjekt 91

Rapport:
FISKEN OG HAVET NR.27 - 1996

Tittel:
APPLICATION OF A HYDRODYNAMICAL MODEL ON TRANSPORT OF LARVAE OF POLAR COD IN THE NORTHERN BARENTS SEA.

Forfatter(e):
Ragnhild Hansen and Bjørn Ådlandsvik

Senter:
Miljø

Seksjon:
Havmiljødata og modellering

Antall sider, vedlegg inkl.:
65

Dato:
14.12.1996

Sammendrag:

Hensikten med denne rapporten er å bruke numerisk modellering til å framskaffe informasjon om gyteområdet til den vestlige komponenten av polartorsk i Barentshavet.

Strømfeltene er laget med en nøstet 3D baroklin strømmodell for Barentshavet med fokus på den nordvestlige delen. Resultatene er sammenlignet med målinger av hydrografi og strømmålinger.

En partikkelsporingsmodell er deretter brukt til å simulere transporten av egg og larver av polartorsk. Resultatene er sammenlignet med fordelingene til de internasjonale 0-gruppeundersøkelsene i Barentshavet. Modellresultatene er konsistente med gyting sørøst for Edgeøya.

Emneord - norsk:
1. Polartorsk
2. Modellering
3. Gytefelt

Emneord - engelsk:
1. Polar cod
2. Modelling
3. Spawning area

Prosjektleder

Seksjonsleder

lk 4997

Application of a hydrodynamical model on transport of larvae of polar cod in the northern Barents Sea.

Ragnhild Hansen and Bjørn Ådlandsvik
Institute of Marine Research
P.O.Box 1870, Nordnes
N-5024 Bergen, Norway

Abstract

The objective of this report is to use numerical modelling to obtain information on the spawning area of the western component of polar cod in the Barents Sea.

A nested 3D baroclinic current model for the Barents Sea with focus on the north-western part is used to provide current fields. The results are compared to hydrographic and current measurements.

A particle tracking model is thereafter used to simulate the transport of eggs and larvae of polar cod. These results are compared to the early juvenile distributions of polar cod from the international 0-group surveys in the Barents Sea. The model results are consistent with spawning southeast of Edgeøya.

CONTENTS

SUMMARY

A nested version of the Princeton Ocean Model has been set up and evaluated for the Barents Sea. The model system consists of a model with 20 km resolution covering the whole Barents Sea together with a 4 km model for the Svalbardbanken area. Input data for the large model is taken from a gridded climatological dataset produced earlier by the Institute of Marine Research (IMR) and The Norwegian Meteorological Institute (DNMI). The 4 km model in turn is driven by the results from the larger model. Meteorological forcing for both models is taken from DNMI's Hindcast Archive.

For evaluation of the model skill, the summer–autumn 1985 and winter 1987–1988 periods have been simulated. The results from the summer simulation are compared to hydrographic measurements taken by IMR under the Pro Mare program, while the winter results are compared to current measurements by Oceanor. The model reproduces the main features of the standard view of the surface circulation. The summer hydrography on Svalbardbanken is complex with strong gradients. The model produces the main water masses in the correct positions, but some of the water mass characteristics are wrong and the fields are too smooth. The winter results show good agreement with the current observations.

The main current in the simulations is the Warm Core Jet flowing into the Barents Sea on the southern flank of Svalbardbanken. This jet follows closely the 250 m isobath. This jet is driven by the Norwegian Atlantic Current. Further up on the bank, the model gives a weaker Bear Island Current flowing in the opposite direction. In the model this current is driven by the density difference between the Arctic and Atlantic water masses. The westwards transport of Arctic Water in the area may be too weak in the model. Other model simulations have shown that the tidal residual current is also important for the Bear Island Current.

A Lagrangian particle tracking model has been developed at IMR. The input data is modelled current fields, here from the 1987–88 simulation. Particles were released southeast of Edgeøya during the winter. A large portion of the particles were lost from the area to the north east of Svalbard. The rest of the particles moved slowly westwards partly on and partly north of Svalbardbanken. As this is one of the main areas for early juvenile polar cod, the model results are consistent with a hypothesis of spawning southeast of Edgeøya. The model was not able to reproduce the 0-group concentrations found each year west of Spitzbergen. This may be due to other spawning areas not included in the model, but are more probably due to the weak transport

of Arctic Water.

Sensitivity studies were performed were the release time and position for the particles varied. The essence of the results is that minor modifications have little influence on the particle distribution in August. The particles stay more or less in the same area and are influenced by the same weather events. A result of the weak sensitivity is that it is not possible to infer the spawning area with high precision on the basis of these modelled current fields.

SAMMENDRAG

En nøstet versjon av Princeton Ocean Model er satt opp og evaluert for Barentshavet. Modellsystemet består av en modell med 20 km oppløsning for hele Barentshavet og en modell med 4 km oppløsning som dekker området omkring Svalbardbanken. Inngangsdata for den store modellen er tatt fra et griddet klimatologisk datasett produsert tidligere av Havforskningsinstituttet (HI) og Det norske meteorologiske institutt (DNMI). Deretter blir 4 km-modellen drevet av resultatene fra den ytre modellen. Meteorologiske drivkrefter for begge modeller kommer fra DNMIs Hindcast arkiv.

To situasjoner, sommer–høst 1985 og vinter 1987–1988, ble kjørt for å evaluere kvaliteten på modellen. Sommerresultatene er sammenlignet med hydrografiske observasjoner tatt av HI i ProMare perioden, mens vinterresultatene sammenlignes med strømmålinger tatt av Oceanor. Modellen reproduserer hovedtrekkene i standardbildet av overflatesirkulasjonen. Sommerhydrografien på Svalbardbanken er svært kompleks med sterke gradienter. Modellen gjenskaper vannmassene på riktig sted men noen av vannmassekarakteristikkene er feil og feltene er for glatte. Vinterresultatene samsvarer godt med strømobservasjonene.

Den dominerende strømmen i simuleringene er den konsentrerte strømmen av Atlanterhavsvann ("the Warm Core Jet") som følger 250 m-koten på sørflanken av Svalbardbanken inn i Barentshavet. Drivkraften her er den Norske Atlanterhavstrømmen. Høyrere opp på banken produserer modellen en svakere Bjørnøyastrøm i retning ut av Barentshavet. I modellen drives denne av tetthetsforskjellene mellom de Atlantiske og Arktiske vannmassene. Modellen underestimerer trolig den vestlige transporten av Arktisk vann i området. Andre modellsimuleringer har vist at tidevannsreststrømmen også er viktig for Bjørnøyastrømmen.

En Lagrangsk partikkelsporingsmodell er utviklet ved HI. Inngangsdataene er modellerte strømfelt, her fra 1987–1988 simuleringene. Partikler ble sluppet ut sørøst for Edgeøya om vinteren. An stor del av partiklene forsvant ut av området norøst for Svalbard. Resten av partiklene fløt langsomt vestover delvis over og delvis nord for Svalbardbanken. Ettersom dette er blant områdene med høyest konsentrasjon av 0-gruppe polartorsk, må modellresultatene sies å være konsistente med en hypotese om gyting sørøst for Edgeøya. Fordelingskartene viser konsentrasjoner av polartorsk vest for Spitzbergen hvert år. Modellen klarte ikke å reprodusere disse konsentrasjonene. Grunnen kan være andre gyteområder som ikke har vært undersøkt med modellen, men mer sannsynlig skyldes det den svake transporten av Arktisk vann.

Det ble også gjennomført følsomhetstudier hvor utslippstid og -sted ble variert. Resultatene herfra viser at mindre modifikasjoner har liten innflytelse på partikkelfordelingen i august. Partiklene holder seg mer eller mindre i samme område og påvirkes av de samme værforhold. En konsekvens av denne svake følsomheten er at det ikke er mulig å på grunnlag av disse modellresultatene å bestemme gytefeltene med stor presisjon.

1. INTRODUCTION

Polar cod (*Boreogadus saida*) plays an important role in the Barents Sea ecosystem. As a pelagic plankton feeder it represents an important link between zoo-plankton and higher levels in the food chain such as marine mammals and sea birds. In the coldest water masses in the Barents Sea, with temperature below 0°C, the polar cod is the dominating plankton feeder.

While adult polar cod is expected to be able to avoid areas influenced by an accidental oil spill, the egg, larvae and juvenile stages may be heavily affected. An overlap in space and time between oil spill and early stages of polar cod may therefore have serious ecological consequences. For this reason it is important to estimate the spawning area and the time evolution of the distribution of eggs and larvae of polar cod.

Existing data on polar cod distribution has been reviewed by Gjøsæter & Anthonypillai (1995). Here the most relevant information comes from the international 0-group investigations, which maps the early juvenile distribution in August, about half a year after spawning. As an example, the distribution in 1988 is shown in figure 1.1. These data confirm that the Barents Sea stock is divided into two components of approximately the same size, one western and one eastern.

The eastern component is reasonably well documented in the Russian literature, an overview can be found in Sameoto (1984). Unfortunately, very little is known on the spawning of the western component. Partially based on information about the eastern component, the western component is expected to spawn under ice in late winter/early spring. As the eggs and larvae are transported with the current system, knowledge of the circulation may help to describe the spawning area. Figure 1.2 from Loeng *et al.* (1995) shows the standard view of the mean surface circulation in the Barents Sea. Combining this information with the 0-group distributions, some areas such as the Atlantic Water mass can be ruled out as spawning area. The Bear Island current, floating towards southwest at the southern flank of the Svalbard bank, is a likely contributor to the observed distributions. If this is the case, the spawning area for the western component may be located somewhere east or south east of Spitzbergen.

To obtain more precise information, further quantitative information on the current picture and the time and depth dependent variability is required. This may be accomplished by the use of numerical current models.

Several model experiments has been done for the Barents Sea. Tidal modelling has been

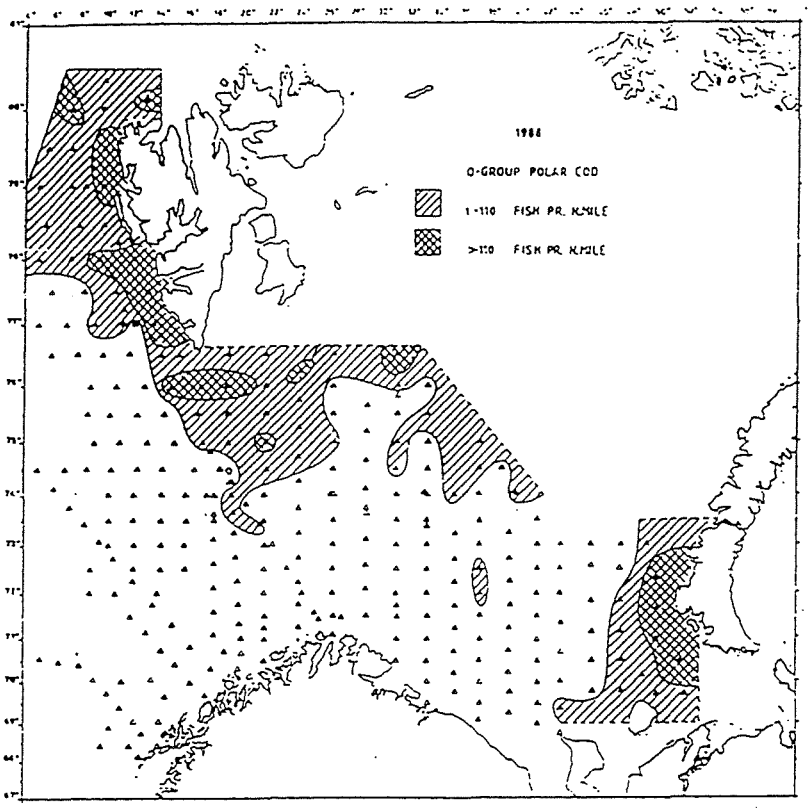

Figure 1.1: Distribution of 0-group polar cod in 1988

performed by Gjevik *et al.* (1990, 1994) and also by Kowalik & Proshutinsky (1995). A wind-driven model was used by Ådlandsvik (1989); Ådlandsvik & Loeng (1991) to study interannual variability in the inflow from the Norwegian Sea. The first modelling of the density driven current were done by Slagstad *et al.* (1990); Støle-Hansen & Slagstad (1991). The work by Slagstad & Støle-Hansen (1991); Slagstad & Stokke (1994) also includes modelling of primary production . Model studies of circulation and bottom water formation in the Barents Sea were done by Harms (1992, 1994). The circulation has also been studied with a laboratory model, McClimans & Nilsen (1993). Two recent Ph.D. theses, Li (1995) and Parsons (1995), include modelling of the Polar Front area south of the Svalbard Bank. In addition there exist several studies on larger scale covering the Barents Sea, with emphasis on the Nordic Seas or the Arctic Ocean.

During the last few years, numerical models have been introduced as a new method for the study of larval transport of fish. Internationally this has been done in the North Sea for herring (Bartsch *et al.*, 1989), sprat (Bartsch & Knust, 1993). At Georges Bank such studies has been performed on cod (Werner *et al.*, 1993). At the Institute of Marine Research (IMR) this method has been used for sandeel in the North Sea (Berntsen *et al.*, 1994), cod in the Barents Sea

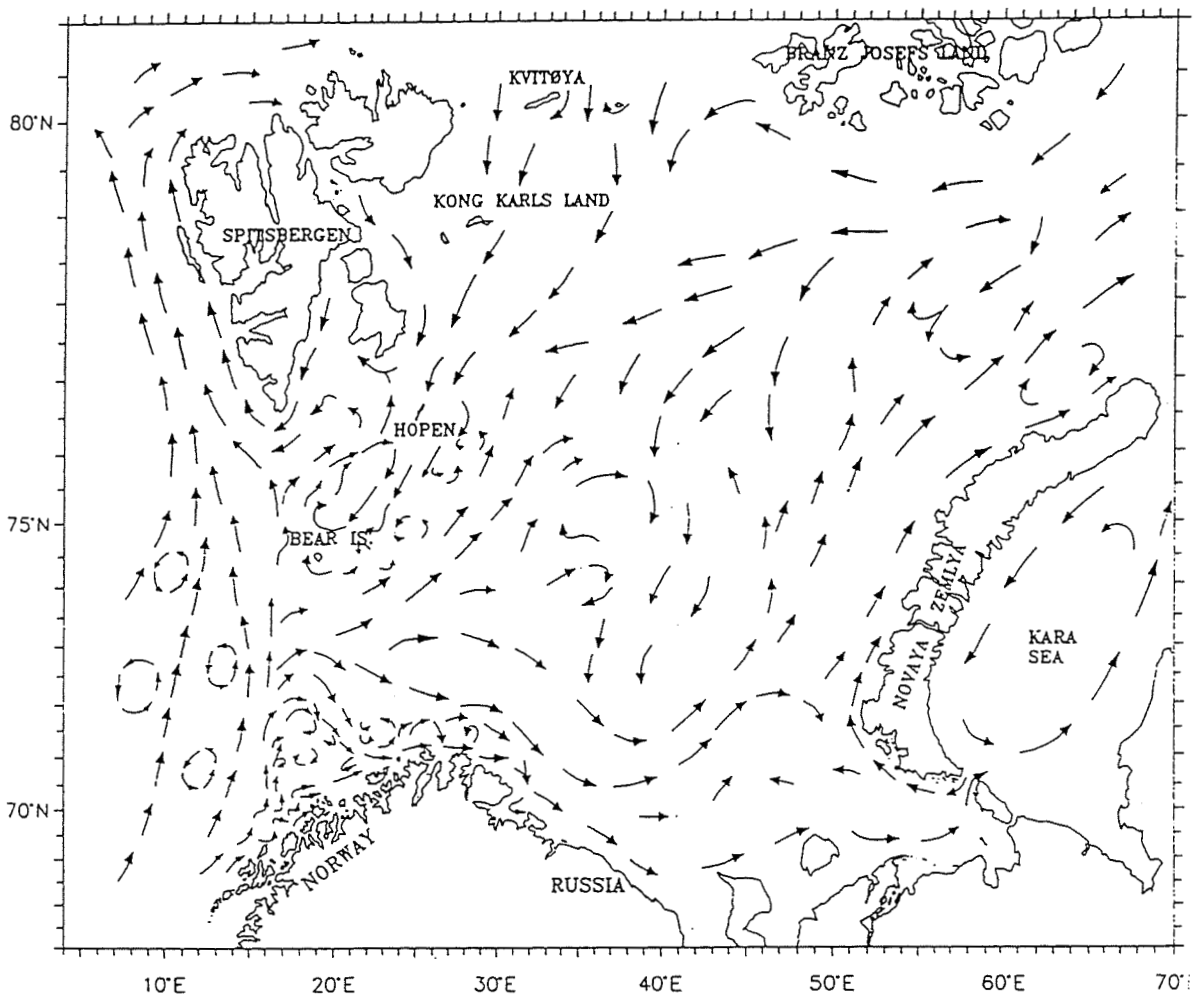

Figure 1.2: Mean surface circulation in the Barents Sea

(Ådlandsvik & Sundby, 1994) and herring larvae in the Norwegian Sea (Svendsen *et al.*, 1995).

These methods combine the use of hydrodynamic current models for the flow field with Lagrangian transport models for tracking particles along flow lines. Additional diffusion can be included by the random walk method.

Due to lack of important physics, numerical problems, poor resolution and inaccurate initial and forcing data the reliability of model results is uncertain. Most of this uncertainty is within the current model. Model results must therefore be thoroughly evaluated before any conclusions can be drawn.

In this work we have applied these techniques to study the transport of eggs and larvae of polar cod in the northern Barents Sea. Here we have used a three-dimensional, baroclinic model, as described in chapter 2. The model is used with a nested set-up, first a relatively course resolution for the whole Barents Sea providing boundary data for a finer resolution model for the Svalbard Bank area.

Chapter 3 presents the input data to the hydrodynamic model and the data used for validation of the model results. The model results is presented in chapter 4, which also contains comparisons with observations on hydrography and currents. Chapter 5 describes the particle transport model and in chapter 6 the results from the transport simulations are shown.

2. DESCRIPTION OF THE HYDRODYNAMICAL MODEL

2.1 Mathematical description

The hydrographic model used is the Princeton Ocean Model (POM), developed by Blumberg & Mellor (1987). This is a three-dimensional, baroclinic numerical model, which calculates salinity, temperature, current fields, surface elevation and two variables connected to vertical mixing. Two simplifications are applied; first the *hydrostatic approximation* and second the *Boussinesq approximation*, which implies that the density, ρ, is replaced everywhere by the mean density, ρ_0, except in the buoyancy term, $-\rho g$ in equation (2.6).

The model consists of the equations of motion for the horizontal velocity field

$$\frac{\partial u}{\partial t} + \mathbf{u} \cdot \nabla u + w\frac{\partial u}{\partial z} - fv = -\frac{1}{\rho_0}\frac{\partial P}{\partial x} + \frac{\partial}{\partial z}[K_m \frac{\partial u}{\partial z}] + F_x \tag{2.1}$$

$$\frac{\partial v}{\partial t} + \mathbf{u} \cdot \nabla v + w\frac{\partial v}{\partial z} + fu = -\frac{1}{\rho_0}\frac{\partial P}{\partial y} + \frac{\partial}{\partial z}[K_m \frac{\partial v}{\partial z}] + F_y \tag{2.2}$$

and the continuity equation

$$\nabla \cdot \mathbf{u} + \frac{\partial w}{\partial z} = 0. \tag{2.3}$$

In the above equations

$\mathbf{u} = (u, v)$	:	Horizontal velocity with components in x- and y-direction
w	:	Vertical velocity component
P	:	Pressure
η	:	Surface elevation
f	:	Coriolis parameter
ρ_0	:	Reference density
K_m	:	Vertical eddy diffusivity
F_x, F_y	:	Horizontal diffusion terms

The model is used in *prognostic mode*, which means that temperature and salinity evolves in time according to the conservation laws

$$\frac{\partial c}{\partial t} + \mathbf{u} \cdot \nabla c + w\frac{\partial c}{\partial z} = \frac{\partial}{\partial z}[K_h \frac{\partial c}{\partial z}] + F_c \tag{2.4}$$

where $c = S$ for salinity and $c = T$ for temperature. K_h is vertical turbulent diffusion of salinity and temperature and F_c is a parametrisation of the horizontal mixing processes.

By using temperature and salinity, density is computed from an equation of state of the form

$$\rho = \rho(S, T) \tag{2.5}$$

The pressure is computed by integrating the hydrostatic approximation to the vertical equation of motion

$$\rho g = -\frac{\partial P}{\partial z} \tag{2.6}$$

where density is given by (2.5).

To calculate the coefficients for vertical mixing, a Mellor-Yamada two-equation turbulence closure scheme is applied (Mellor & Yamada, 1982).

As boundary condition at the surface, we use that the vertical velocity shear of the current vector is proportional to the wind stress, that means

$$\rho_0 K_m(\frac{\partial u}{\partial z}, \frac{\partial v}{\partial z}) = (\tau_{0x}, \tau_{0y}) \tag{2.7}$$

where (τ_{0x}, τ_{0y}) is the wind stress vector at the surface. There is a similar condition at the bottom, where the bottom stress is used. For Equation (2.4) the boundary condition is

$$\rho_0 K_h(\frac{\partial T}{\partial z}, \frac{\partial S}{\partial z}) = (\dot{H}, \dot{S}) \tag{2.8}$$

where $\dot{H}$ is the net ocean heat flux and $\dot{S} = S(0)(\dot{E} - \dot{P})/\rho_0$ with $\dot{E} - \dot{P}$ the net evaporation-precipitation fresh water surface mass flux rate and $S(0)$ the surface salinity. There is no heat or salt flux across the bottom boundaries.

At coastline boundaries the velocities normal to the land are set to zero. At the open boundaries the "Flow Relaxation Scheme" (FRS) has been used. This method were introduced to ocean modelling by Martinsen & Engedahl (1987) and later implemented in POM Engedahl (1995). This means that every prognostic variable is updated by the linear combination $\phi = (1 - \beta)\phi_{int} + \beta\phi_{ext}$, where ϕ_{int} is the time integrated, non relaxed solution at the model area and ϕ_{ext} a specified external solution in the FRS-zone. β is a relaxation parameter which varies from zero to one throughout the FRS-zone. Here the external solution is defined by the climatological field-variables and the updating is done at every time step.

2.2 Numerical solution techniques

In the vertical a sigma-coordinate representation is used. This means that the vertical coordinate is scaled by the depth of the water column

$$\sigma = \frac{z - \eta}{H + \eta} \tag{2.9}$$

where $H(x, y)$ is the bottom topography and $\eta(x, y)$ the surface elevation. This leads to a better representation of the bottom topography and a more simple treatment of the boundary conditions. For the transformation of the model equations to the sigma coordinate system, see Blumberg & Mellor (1987).

The horizontal finite differencing scheme uses Cartesian coordinates in a staggered grid. In the literature this has been called an Arakawa-C grid.

Equations (2.1)-(2.4) are solved by a time splitting technique, where fast moving surface gravity waves are separated from slow moving internal gravity waves. This technique avoids the usual small time steps associated with the fast moving gravity waves. In the vertically integrated, external mode part of the equations the time step is limited according to the CFL-condition

$$\Delta t \leq \frac{1}{C_t}(\frac{1}{\Delta x^2} + \frac{1}{\Delta y^2})^{-1/2} \tag{2.10}$$

where $C_t = 2(gH)^{1/2} + U_{max}$, U_{max} being the maximum average current velocity expected. The internal mode time step is limited according to the rule

$$\Delta t \leq \frac{1}{C_T}(\frac{1}{\Delta x^2} + \frac{1}{\Delta y^2})^{-1/2} \tag{2.11}$$

where $C_T = 2\,C + U_{max}$, where U_{max} is the maximum advective speed and C the maximum internal gravity wave speed. This requirement is much less stringent, since the fast moving external gravity effects have been removed.

The internal mode calculations are separated into a vertical diffusion time step, which is carried out implicitly, and an explicit advection plus horizontal diffusion time step. This may be illustrated by the sigma coordinate version of the temperature equation (2.4), see also Mellor (1995).

$$\frac{\partial(TD)}{\partial t} + \frac{\partial(TuD)}{\partial x} + \frac{\partial(TvD)}{\partial y} + \frac{\partial(Tw)}{\partial \sigma} = \frac{\partial}{\partial \sigma}[\frac{K_H}{D}\frac{\partial T}{\partial \sigma}] + DF_T \tag{2.12}$$

which may be written

$$\frac{\partial(TD)}{\partial t} + Adv(T) - Dif(T) = \frac{1}{D}\frac{\partial}{\partial \sigma}[K_H\frac{\partial T}{\partial \sigma}] \tag{2.13}$$

where $D = H + \eta$. The advection and horizontal diffusion parts in (2.13) are differenced according to

$$\frac{D^{n+1}\tilde{T} - D^{n-1}T^{n-1}}{2\,\Delta t} = -Adv(T^n) + Dif(T^{n-1}) \tag{2.14}$$

and the vertical diffusion part is differenced as

$$\frac{D^{n+1}T^{n+1} - D^{n+1}\tilde{T}}{2\,\Delta t} = \frac{1}{D^{n+1}}\frac{\partial}{\partial\sigma}[K_H\frac{\partial T^{n+1}}{\partial\sigma}] \tag{2.15}$$

This technique permits the use of fine vertical resolution in the surface and bottom boundary layers without drastically reducing the time step, as would be the case with an explicit scheme.

The external mode equations are entirely explicit. This means that all vertical differencing is implicit whereas all horizontal differencing is explicit.

2.2.1 Model parameters

The operation of the model is partially governed by a set of parameters. The most important for this work are discussed below.

`umol` is a minimum value for the vertical eddy viscosity coefficient, which is calculated by the turbulence closure model. In most of the simulations we have taken `umol` = 2×10^{-5} m^{2}s^{-1}. The model also has the possibility of keeping the vertical eddy viscosity coefficient constant throughout the grid. This is done by taking the input parameter `noclose = .TRUE.`, which excludes the turbulence scheme calculations.

`horcon` is a dimension-less constant in the Smagorinsky diffusion formula for the horizontal eddy diffusivity

$$A_M = \texttt{horcon} \cdot \Delta x\,\Delta y\,\frac{1}{2}\,|\nabla V + (\nabla V)^T| \tag{2.16}$$

Here `horcon` is usually of size 0.1. Too small value of `horcon` may lead to instabilities while too large value will produce unrealistically smooth fields.

`metforce`, `clima`, `rivers` and `tide` controls the imposing of meteorological forcing, climatological input, river inflow and tidal forces, respectively. Maximum number of tidal constituents are 8.

`climintpol = .TRUE.` gives the possibility of time interpolation of climatological input fields or input fields for nesting.

`rnewmin` and `rnewmax` are the minimum and maximum allowed sea depths. Here we had to increase `rnewmin` to the order of 10–20 m to avoid stability problems.

`surfrel` is a logical switch for deciding whether to relax the surface density field towards the climatological field. This is done by adding the correction terms

$$\texttt{wtsurf} = -\texttt{fluxcoef}\,(T_{cli} - T) \tag{2.17}$$

$$\texttt{wssurf} = -\texttt{fluxcoef}\,(S_{cli} - S) \tag{2.18}$$

to the temperature and salinity equations (2.4) at the surface boundary. T_{cli} and S_{cli} are the climatological values, and T and S are the surface variables as predicted by the model.

This will force the model-predicted surface variables towards the climatological values and e.g give winter cooling and fresh water if the actual climatological field is imposed every month during the winter period.

`fluxcoef` is the Newtonian coefficient of the surface fluxes of temperature and salinity. Here `fluxcoef` = $1.736 \times 10^{-5}\,\mathrm{ms}^{-1}$.

Finally we mention that the model may be used both in prognostic and diagnostic modes, which is controlled by the parameter `mode`. In the *prognostic* mode (`mode=3`) both the momentum and conservation equations are integrated as an initial value problem. These experiments do not always reach steady state, since the oceanic response time for the density field can be large. In the *diagnostic* calculations (`mode=4`) temperature and salinity are specified at all points in the grid and held fixed in time. These experiments typically attain steady state after 10 days and may be used to initialise a prognostic forecast model. The model also has the possibility to be used in two dimensions only (`mode=2`), which means that no internal equations are solved.

3. DATA FOR HYDRODYNAMIC MODELLING

This chapter gives a short description of the oceanographic data used as initial and boundary conditions for the hydrodynamic model and the data that will be compared with the model results.

3.1 Oceanographic initial and boundary data

In two projects IMR and the Norwegian Meteorological Institute (DNMI) have developed monthly climatological descriptions of hydrography, sea surface elevation and currents for Norwegian waters including the Barents Sea. The latest versions are documented in (Engedahl *et al.*, 1995). The temperature, salinity and current fields are given at 31 standard depth levels.

The starting point was Levitus' global climatology (Levitus, 1982) of salinity and temperature. This data set was interpolated in space to a 20 km grid and in time to monthly fields. This data set was enhanced by North Sea data (Damm, 1989) and measurements taken by IMR in the Norwegian and Barents Seas. For each month the resulting hydrographic data set was kept fixed while the model was spinning up with climatological wind forcing. This hydrography together with the resulting sea surface elevation and current fields constitute the *diagnostic climatology*. Based on this archive, the model was run prognostically (i.e. salinity and temperature evolved in time according to equation (2.4)) for seven years with realistic wind forcing and river runoff. The resulting data sets for each month of the last year constitutes the *prognostic climatology*.

The prognostic climatology is more detailed and has evolved nice fronts in certain areas. In other areas, including the Barents Sea, the hydrography has drifted away from the observed values. It is more uncertain which current field is the best. For the simulations reported here the diagnostic climatological archive has been used.

The 20 km model has also been run with M_2 tidal forcing. These data were taken from model results of Gjevik's group (Gjevik *et al.*, 1990). Tidal forcing is not included in the results reported here. As the model area is not close to any major river, river runoff has also been neglected. As the present version of the model does not include ice, ice data has been neglected.

3.2 Meteorological data

The atmospheric forcing, wind stress and air pressure, is taken from the Hindcast archive of DNMI (Eide *et al.*, 1985). This archive consist of 6-hourly analysed fields from 1955 to present on a 75 km grid. The archived variable is the height of the 1000 mbar surface, from which wind stress and surface air pressure are computed.

No atmospheric data are used for heat transfer between the ocean and atmosphere. To account for the seasonal temperature cycle, the discrepancy between the sea surface temperature in the model and the climatology is used to calculate a heat flux by equation (2.17).

3.3 Data for comparison

To assess the quality of the results from the model, the results must be compared to other knowledge, preferably real observations. It is generally difficult to compare an observation at one point in space and time with the corresponding result from the model. It is better to compare more integrated values or views such as 2D sections, horizontal or vertical. The observations used here are hydrographic sections from CTD-measurements and the current component normal to an array of moored current meters.

The observations in the area are somewhat biased since almost all CTD-casts on Svalbardbanken are taken during the summer and autumn seasons under ice-free conditions. The model comparison runs has been done for the same periods, and may therefore not be fully representative for the period of drifting eggs of polar cod.

The best hydrographic coverages of Svalbardbanken were performed during the Pro Mare period (1984–89). A number of hydrographic sections, here called PM1 – PM4, were covered several times. These sections are showed in Fig. 3.1 and the positions of their endpoints are given in table 3.1. The best coverage was in August 1985 with R/V "G.O. Sars" as documented in the cruise report (Loeng, 1986). The section PM2 was not covered on this cruise.

PM1	(75°15′N, 21°08′E)–(74°07′N, 24°42′E)
PM2	(75°15′N, 15°00′E)–(75°15′N, 21°08′E)
PM3	(75°15′N, 21°08′E)–(75°15′N, 28°40′E)
PM4	(76°30′N, 25°20′E)–(75°15′N, 28°40′E)

Table 3.1: The end points of the Pro Mare sections

There have been some current measurements in the area. The most suitable data come from an array of 5 moorings from November 1987 to April 1988. These measurements were carried

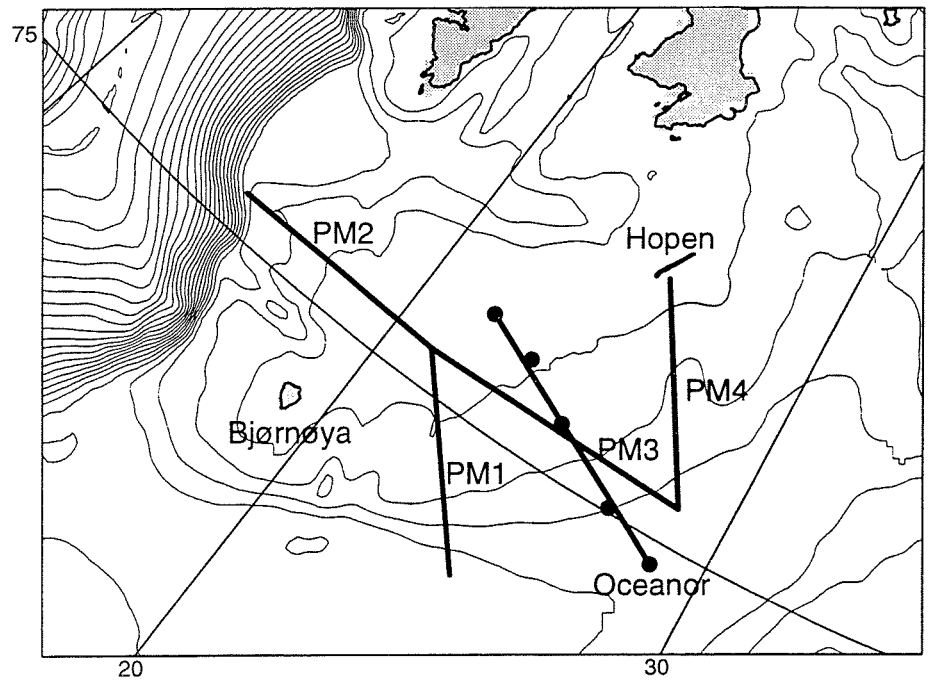

Figure 3.1: Map showing the vertical sections, the current meter positions and bottom contours for every 100 m

out by Oceanor and is reported in Johansen *et al.* (1988) and further analysed by Loeng & Hansen (1997). The positions of the current meters are given in table 3.2. The positions are also mapped as black discs in Fig. 3.1 and the section is here simply named Oceanor.

S1	75°40′N	21°57′E
S2	75°34′N	23°26′E
S3	75°20′N	25°00′E
S4	75°02′N	25°07′E
S5	74°51′N	28°43′E

Table 3.2: Positions of the OCEANOR moorings

4. SET-UP AND VALIDATION OF THE HYDRODYNAMICAL MODEL

4.1 Nested set-up

A map of the model domain is shown in fig. 4.1. It stretches from Svalbard and Franz Josef Land in the north to the White Sea in the south. Inside this domain there is a smaller nested domain covering Svalbardbanken, this subdomain is marked with a rectangular frame in the map. For the outer domain a relatively coarse resolution of 20×20 km is used, while the nested domain has a resolution of 4×4 km.

Start and boundary data for the 20 km model are taken from the monthly diagnostic climatology described in section 3.1. Daily averaged results from the 20 km model are used as start and boundary data for the 4 km model. The flow relaxation scheme (FRS) is used to pass the boundary information into the models.

The model is run with 6 hourly imposed wind data and river inflow is neglected. In most of the simulations `horcon`=0.1 and `umol`= 2×10^{-5} m^{2}s^{-1}, if not, it will be explicitly specified. According to Mellor (1995) a numerically acceptable minimum depth has not yet been established, but a lower limit of `rnewmin`=10-20 m is a general choice. To get satisfactory results, we had to set a minimum sea depth in this range. A σ-coordinate representation with 10 layers is used and chosen such that higher resolution is achieved near the surface.

The standard parameters in these runs are given by

Large area resolution	:	20 km
Small area resolution	:	4 km
Number of grid-cells in large area	:	95×95
Number of grid-cells in small (nested) area	:	150×110
Internal time step 20 km model	:	900 s
External time step 20 km model	:	30 s

Internal time step 4 km model	:	600 s
External time step 4 km model	:	6 s
σ-layers	:	0.0, -0.002, -0.01, -0.075, -0.15,
		-0.3, -0.5., -0.7, -0.95, -1.0

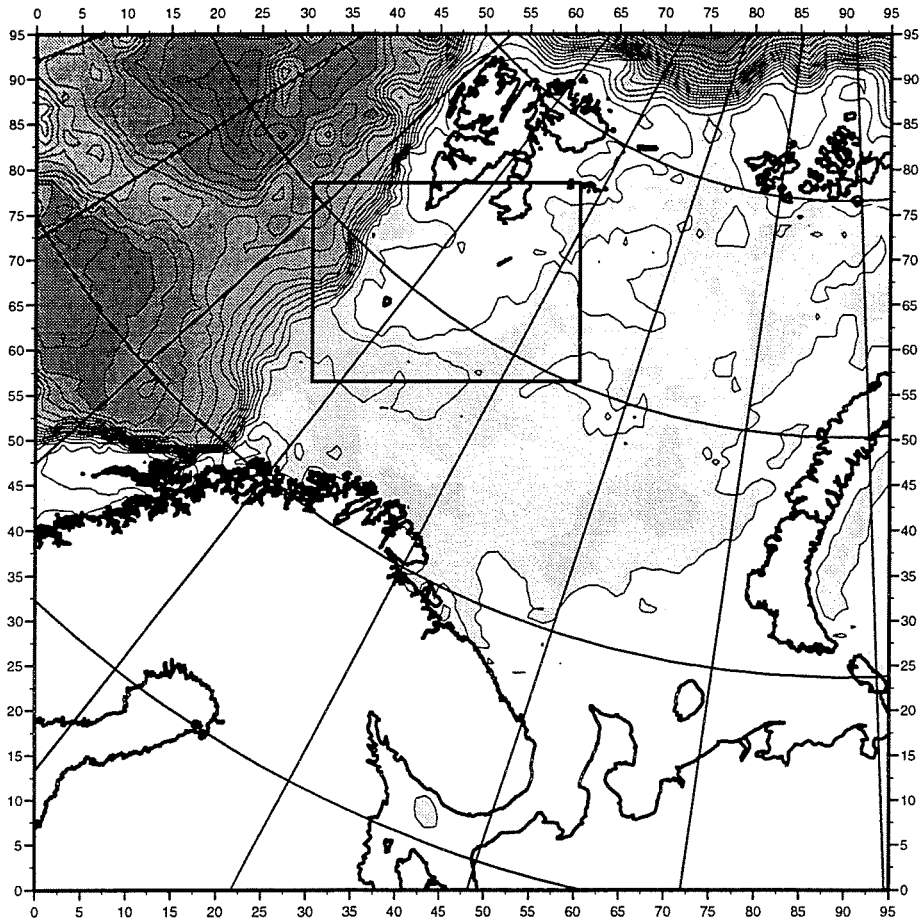

Figure 4.1: Model domains for coarse and fine scale model. Bottom topography is indicated by shading and bottom contours every 200 m.

4.2 Horizontal current fields

As a start, the hydrodynamic model was set up for the large area only. The model was run throughout the months of July, August, September, October and November 1985. This period was chosen to match the Pro Mare data set described in Loeng (1986). The simulation was done without tides and the minimum sea depth `rnewmin` was set to 20 m.

Figure (4.2a) shows the modelled current in the larger domain at 10 m depth averaged over the period July-November 1985. Compared to the standard picture, fig. 1.2, many features of the surface circulation is reproduced. The Norwegian Atlantic Current continues along the shelf edge as the Spitzbergen Current. A fraction enters the Barents Sea in the Bear Island Channel. There is also an inflow close to the Finnmark/Kola coast. Most of the outflow from the Barents Sea leaves through the strait between Novaya Zemlya and Franz Josef Land. In the northwestern Barents Sea the current is quite weak. The Bear Island current towards southwest along the southern slope of Svalbardbanken is not clearly reproduced.

The results from the 4 km simulation, fig. 4.2b, show considerable more details. Except for the Spitzbergen Current the strongest current pattern is the inflow outside the 200 m isobath along the southern slope of Svalbardbanken. This current, named the Warm Core Jet, is somewhat narrower than the Atlantic inflow in the standard view. It is present in the laboratory simulation by McClimans & Nilsen (1993) and has been extensively studied by Li (1995).

Further up on the slope at approximately 100 m bottom depth there is a weaker Bear Island Current flowing towards southwest. This current links the strong anticyclonic circulation around Hopen and the weaker circulation around Bjørnøya. This current seems somewhat weaker than indicated in the standard view.

South of the Warm Core Jet, the model produces a recirculation cell of Atlantic Water. This feature is not in the standard view, but has been observed in other model simulations, (Slagstad *et al.*, 1990; Parsons, 1995). The current field also shows a number of eddies, most of them anticyclonic. As this is an averaged picture over a couple of months, these eddies are quite stationary and are probably caused by topographic steering.

Figure (4.3) shows the current field at 50 m in both resolutions. In the coarse resolution the current is somewhat weaker but quite similar to the 10 m results. A flow towards southwest is now visible at the southern slope of Svalbardbanken. In the 4 km results the Warm Core Jet is weaker in 50 m than near surface, and the Bear Island outflow up on the slope is stronger. Most of the eddies from the 10 m results are still present in the 50 m field, as would be expected from stationary topographic eddies.

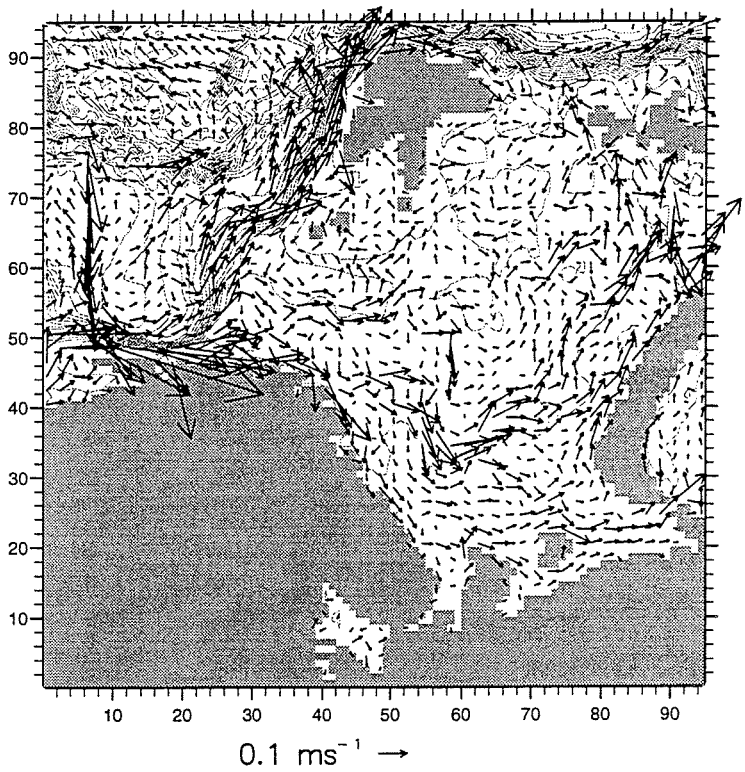

(a) Average of 20 km current field at depth 10 m.

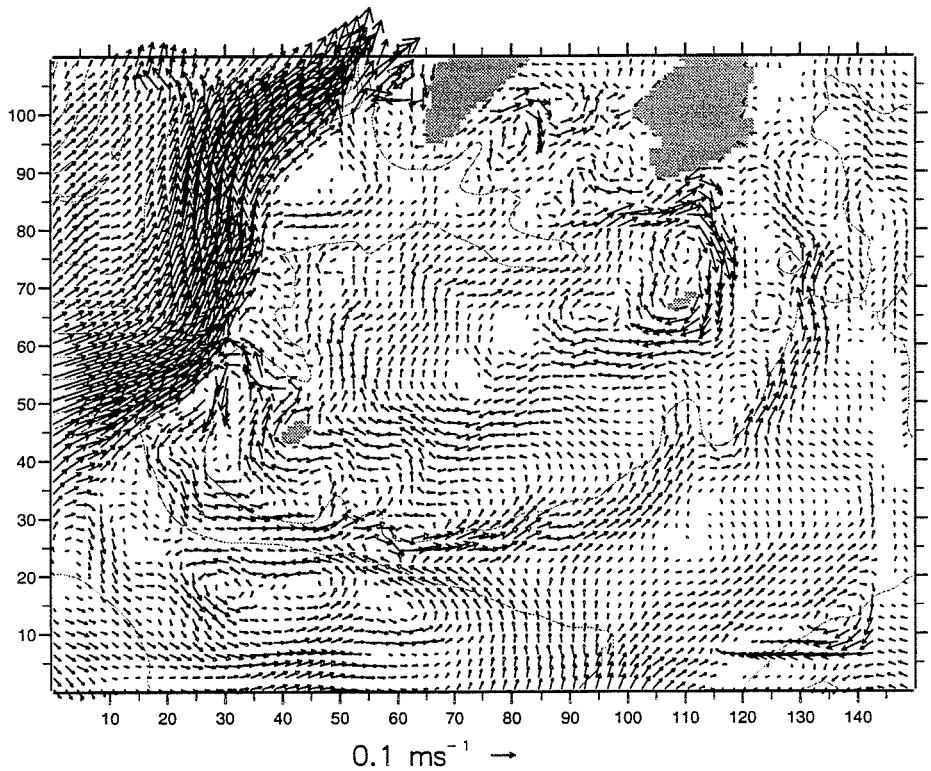

(b) Average of 4 km current field at depth 10 m.

Figure 4.2: Mean current fields for a period of 150 days, starting at 1 July 1985.

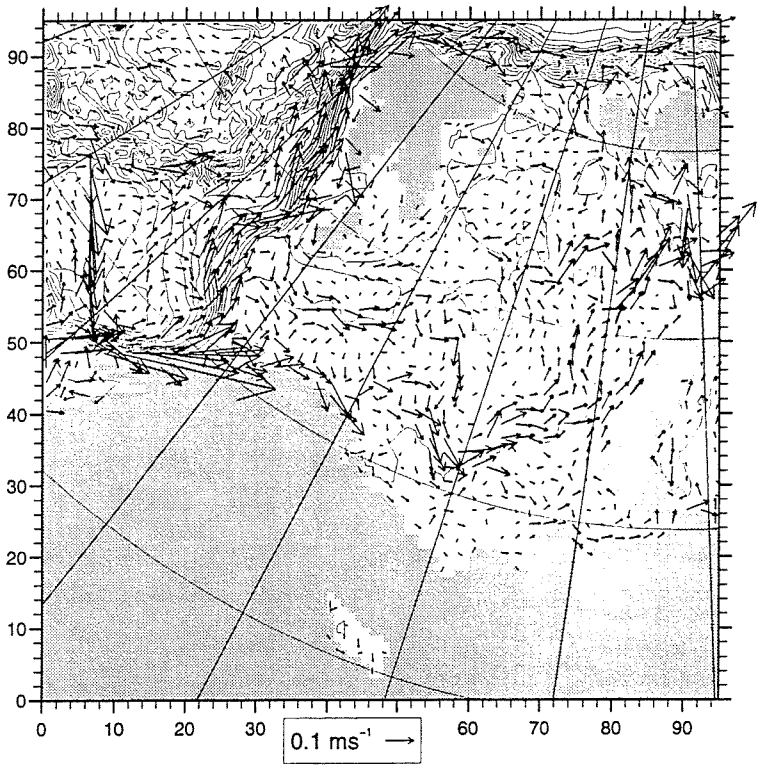

(a) Average of 20 km current field at depth 50 m.

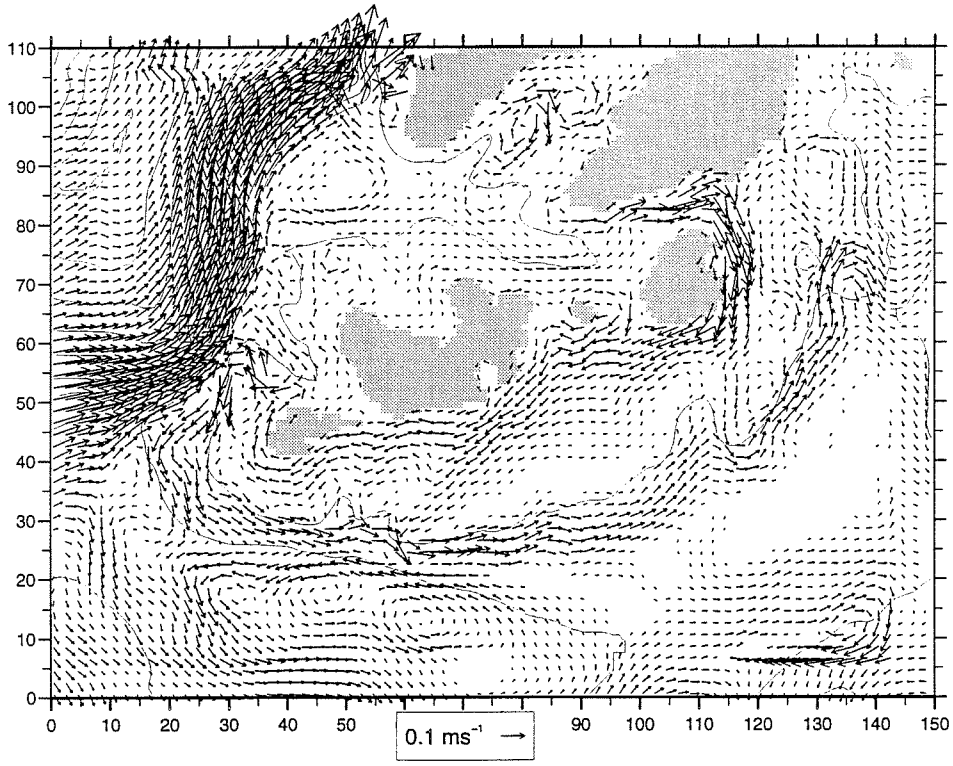

(b) Average of 4 km current field at depth 50 m.

Figure 4.3: Mean current fields for a period of 150 days, starting at 1 July 1985.

4.3 The Pro Mare sections

To assess the performance of the model, model results from the Pro Mare sections (section 3.3) were extracted and plotted. The results presented here include some examples on the sensitivity to the mixing parameters and comparison of model results and observations.

The model was run throughout the period of July to November 1985. Since there are relatively small variations in the modelled data along the sections during the current months, we content ourselves to present the August data only. Temperature, salinity and density are those variables which most easily can be compared to the measured data.

4.3.1 Sensitivity to mixing parameters

Using a hydrodynamic ocean model it is important to choose the right values for the mixing parameters. High mixing gives numerically stable results but the results are unrealistically smoothed. Low mixing might give numerical problems but better results when it can be applied.

Before choosing the parameters, four test runs were performed. The purpose was to examine the sensitivity of the model results to changes in the parameters `horcon` for horizontal and `umol` for minimal vertical mixing. the model. The values of `horcon` and `umol` are given in table 4.1 below.

Run	`horcon`	`umol` [m^2s^{-1}]
a	0.1	2×10^{-5}
b	0.02	2×10^{-5}
c	0.1	2×10^{-4}
d	0.1	2×10^{-6}

Table 4.1: Mixing parameters used in the sensitivity examples

The monthly mean salinity values for August 1985 along the section PM1 are given in fig 4.4. For comparison the observed values in the section is presented in fig 4.6. The results from run (a), (b) and (d) are similar with water fresher than 34.3 at the surface over Svalbardbanken. In run (c) with highest vertical mixing the surface water is more saline and the stratification less pronounced. In the deeper part all runs gave similar results, but there is no salinity above 35.2 in run (c).

The temperature results are shown in figure 4.5. All four runs gave the coldest water near the bottom at approximately 100 m. Somewhat surprisingly, run (b) with lower horizontal diffusivity has no water colder then 0.5°C. In run (d) with lowest vertical mixing there is water below

0°C. Run (c) is here considerably less stratified than the other runs. In the deeper part, the differences are less pronounced. Here too, run (c) produced smoother results. Run (d) gave higher temperature both at surface and bottom in the southern part.

Summing up, the alternative (c) with highest mixing gave the smoothest results. Too low mixing values might lead to instabilities. Therefore the more robust choice (a) is preferred to (b) or (d).

4.3.2 Comparison with hydrographic observations

Figure 4.6 (a), (b) show the measured salinity and temperature fields along section PM1 in August 1985, (c) and (d) show the climatological fields from July used as the initial condition for the simulation and finally (e) and (f) show the model mean fields from August 1985.

For salinity, the measured and climatological section agrees quite well, with the climatology somewhat smoother. The model results are considerable smoother and in particular lacks the fresh surface water over the bank.

For temperature, the difference between the climatology and the measurements are larger. The climatology is colder in the surface off the bank and the very cold water on the bank is missing. The model results are even smoother than the 20 km climatology. The model reproduces the temperature minimum in the correct area, but the temperature minimum is far to high as all water with temperature less than 0°C has disappeared.

Figure 4.7 show the modelled and observed σ_T-values. The density structure reveals the same picture, the pycnocline is unrealistically smooth and the lightest water has disappeared.

The modelled salinity and temperature fields along section PM2 is presented in fig. 4.8. Unfortunately no observations are available for this section in August 1985. In this section the water is mixed to the bottom at the top of the bank. West of the bank the Atlantic Water moving towards Spitzbergen is reproduced in the model.

Figures 4.9 and 4.10 show the modelled and observed salinity and temperature fields from sections PM3 and PM4. The tendency is the same. The model results are too smooth. Temperature and salinity minima are reproduced in the correct areas but the values are too high.

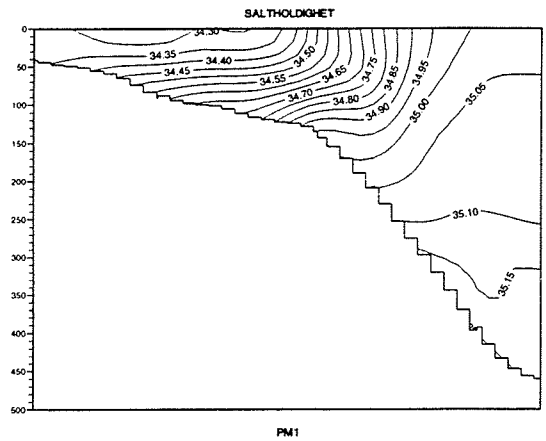

(a) horcon=0.1, umol=2×10^{-5} m^2s^{-1}

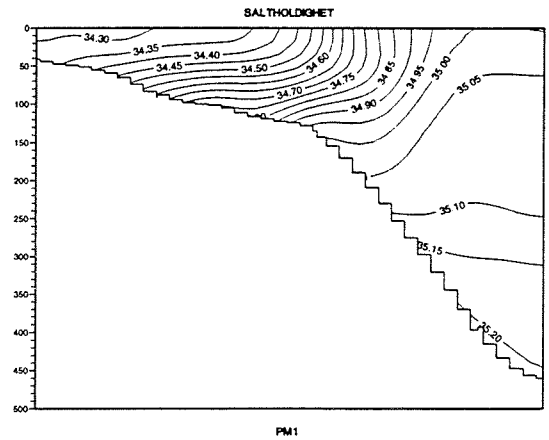

(b) horcon=0.02, umol=2×10^{-5} m^2s^{-1}

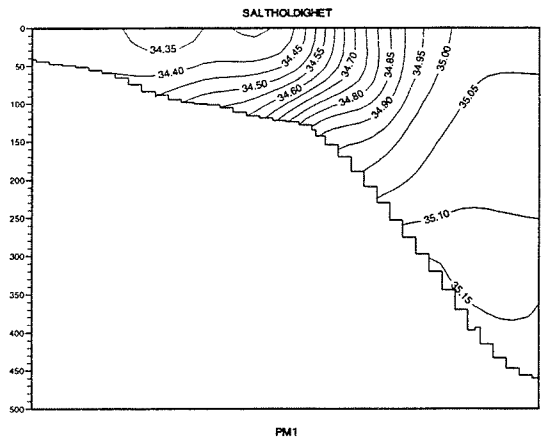

(c) horcon=0.1, umol=2×10^{-4} m^2s^{-1}

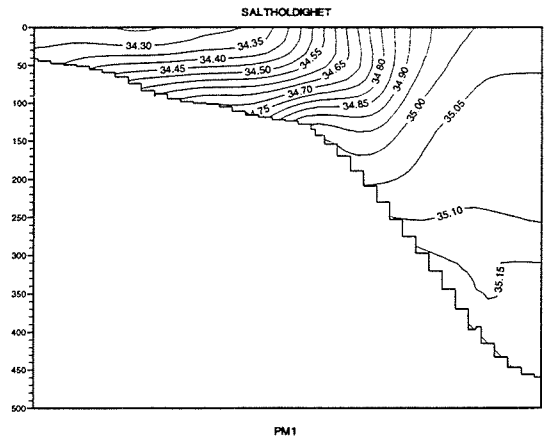

(d) horcon=0.1, umol=2×10^{-6} m^2s^{-1}

Figure 4.4: Modelled mean salinity along section PM1 in August 1985 for different values of horcon and umol.

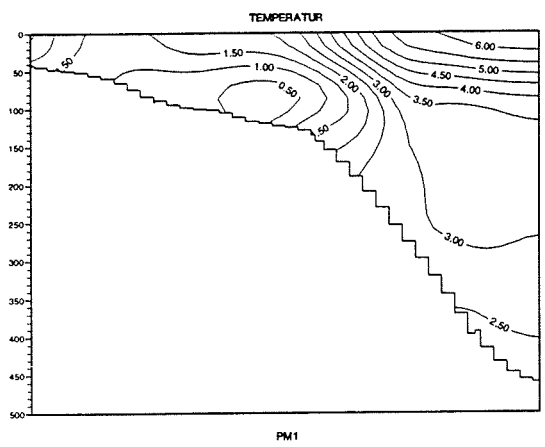

(a) horcon=0.1, umol=2×10^{-5} m^{2}s^{-1}

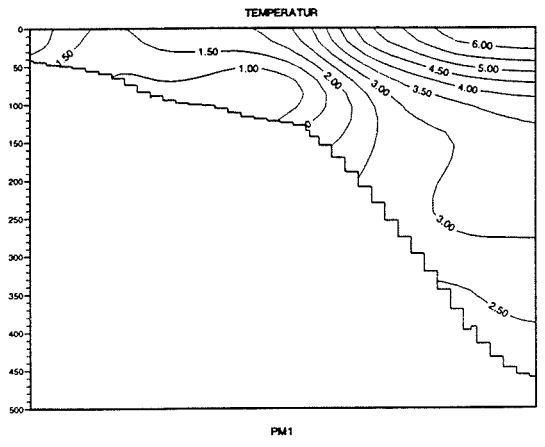

(b) horcon=0.02, umol=2×10^{-5} m^{2}s^{-1}

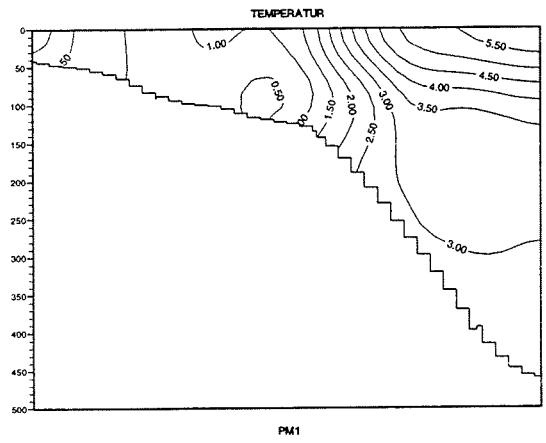

(c) horcon=0.1, umol=2×10^{-4} m^{2}s^{-1}

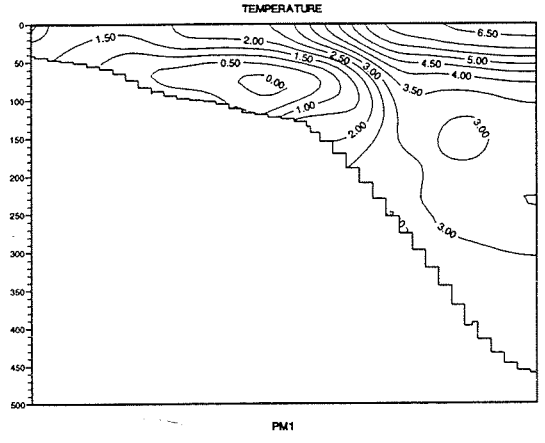

(d) horcon=0.1, umol=2×10^{-6} m^{2}s^{-1}

Figure 4.5: Modelled mean temperature along section PM1 in August 1985 for different values of horcon and umol.

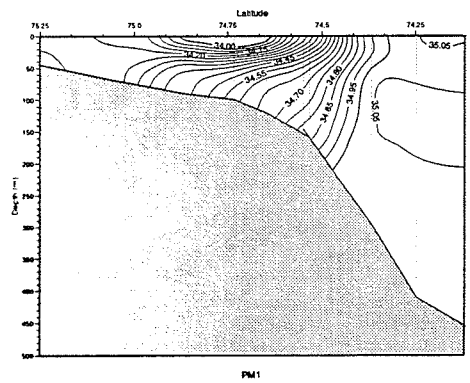

(a) Measured Salinity

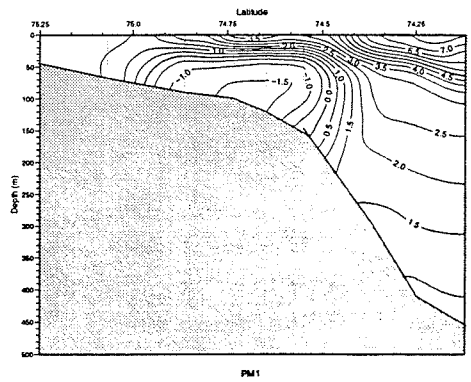

(b) Measured Temperature

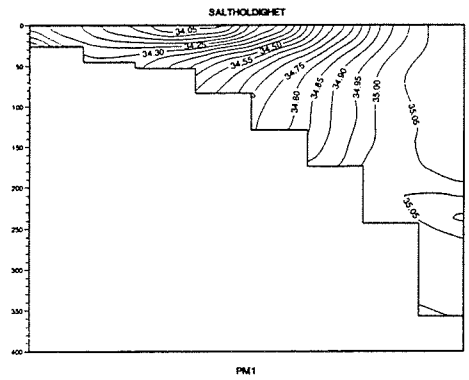

(c) Climatological Salinity

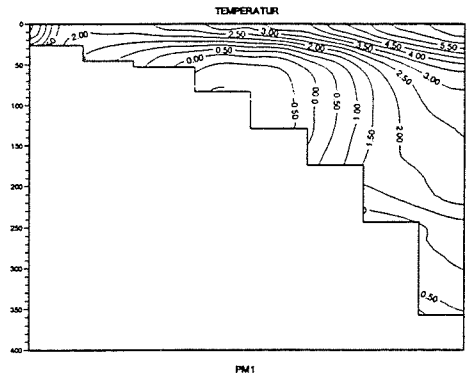

(d) Climatological Temperature

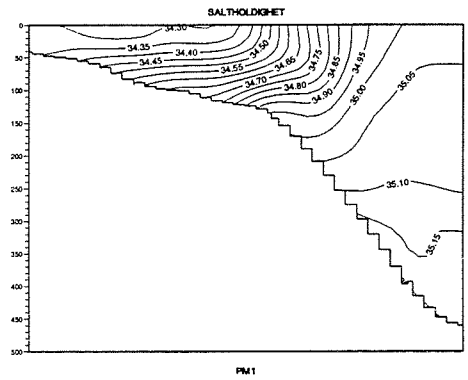

(e) Modelled Salinity

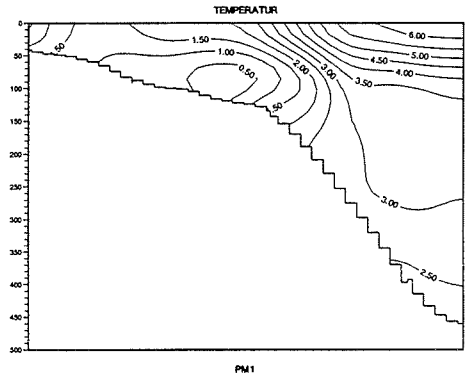

(f) Modelled temperature

Figure 4.6: Salinity, temperature along section PM1, observations from August 1985, July climatology and averaged model results for August 1985.

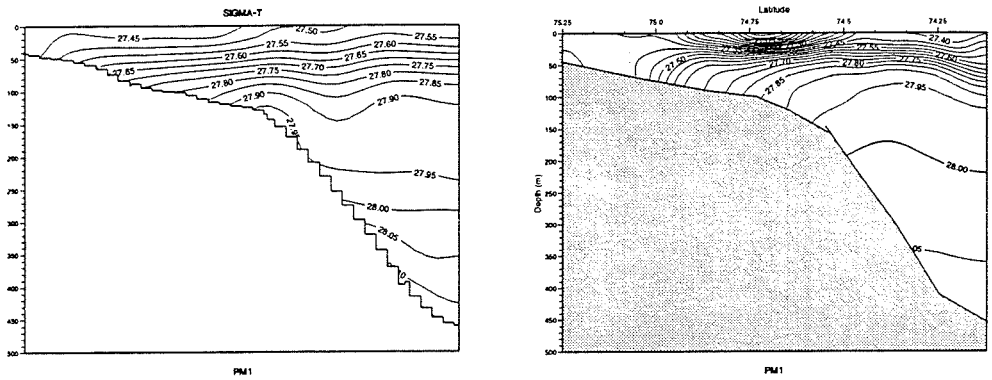

(a) Modelled sigma-T (b) Measured sigma-T

Figure 4.7: Density along section PM1 for the month of August 1985.

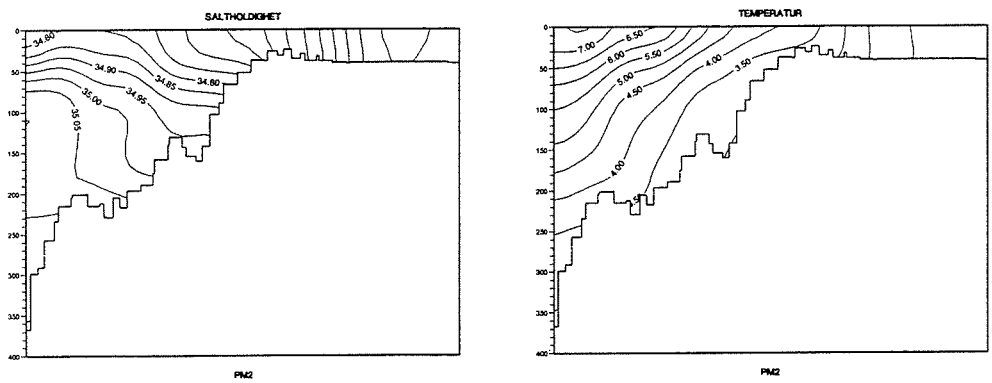

(a) Model salinity (b) Model temperature

Figure 4.8: Salinity and temperature along section PM2 for the month of August 1985.

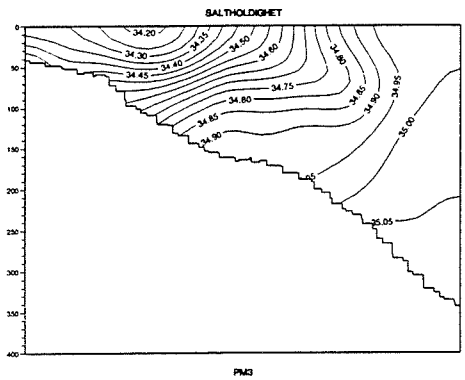

(a) Modelled salinity

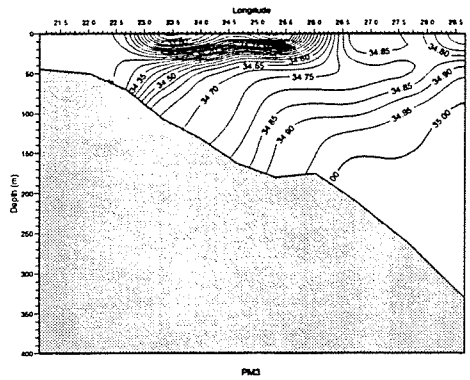

(b) Measured salinity

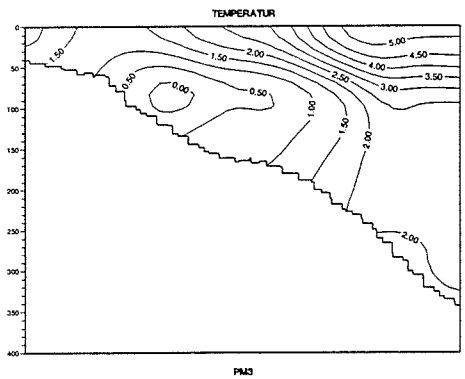

(c) Modelled temperature

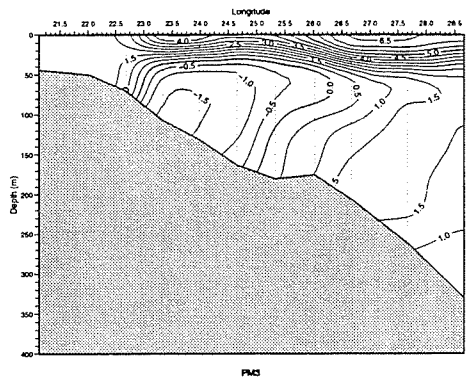

(d) Measured temperature

Figure 4.9: Salinity and temperature along section PM3 for the month of August 1985.

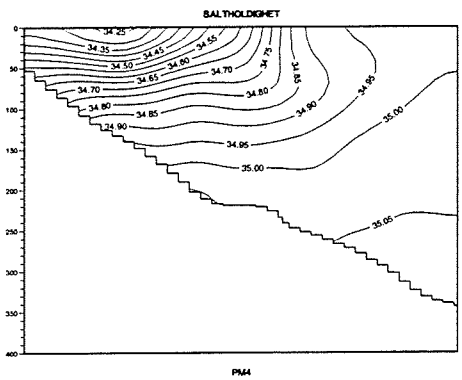

(a) Modelled salinity

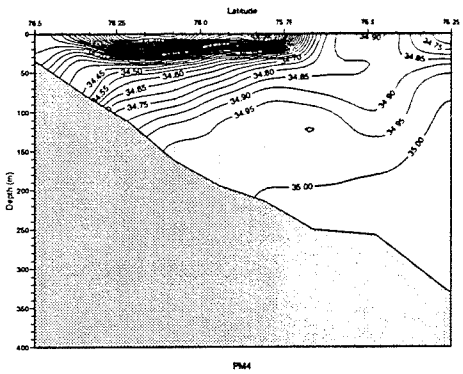

(b) Measured salinity

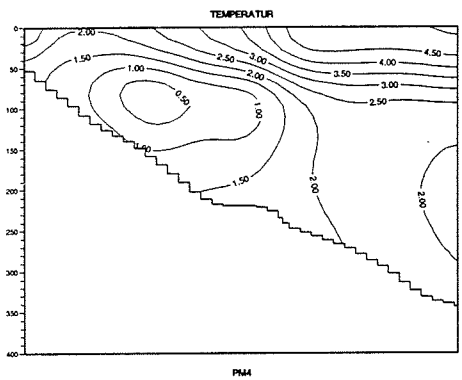

(c) Modelled temperature

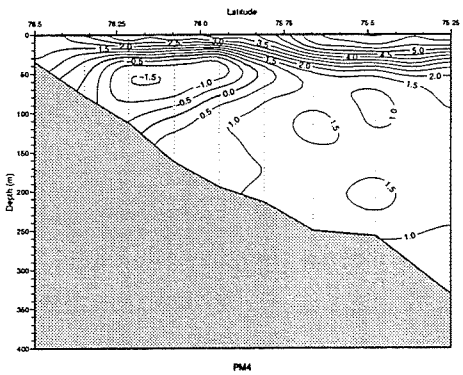

(d) Measured temperature

Figure 4.10: Salinity and temperature along section PM4 for the month of August 1985.

4.4 Comparison with current meters

A nested simulation for the winter 1987–1988 has been performed for comparison with the current measurements by Oceanor described in section 3.3. The model was run throughout the months of October 1987 to February 1988. In this simulation the vertical mixing was set to $\texttt{umol} = 2 \times 10^{-4}\,\mathrm{m^2 s^{-1}}$ and the horizontal diffusion was given by $\texttt{horcon} = 0.1$. To recreate the winter cooling, the surface temperature and salinity were relaxed towards climatology as described in eqs. (2.17) and (2.18).

The horizontal distribution of temperature at 10 m depth for the months of November 1987 to February 1988 are presented in figure 4.11. After the first month the Polar Front has been considerable sharpened by the model. At the right end of the January and February results a strong front has been created. This is an artifact in the FRS zone (section 2.1) caused by mismatch between the 20 km and 4 km results. Figure 4.12 shows the hydrographic structure along the Oceanor section. As expected in winter, the vertical stratification is very weak. A temperature maximum is found over the 300 m isobath corresponding to the Atlantic inflow. On the bank the temperature values are clearly to high.

The monthly mean current component normal to the Oceanor section is depicted in figures 4.13-4.14. The observed current pictures are estimated from the measurements by Loeng & Hansen (1997).

The positioning of the currents in the model agrees very well with the measurements. Both the model results and the data show he Warm Core Jet flowing into the picture over the 250 m isobath and the Bear Island Current flowing out over the 100 m isobath. From November to December this Warm Core Jet became more narrow. This is reproduced by the model. In January and February the currents becomes too strong in the model. South of the jet, the current meters indicate out-flowing water. In January and February this is also present in the model results.

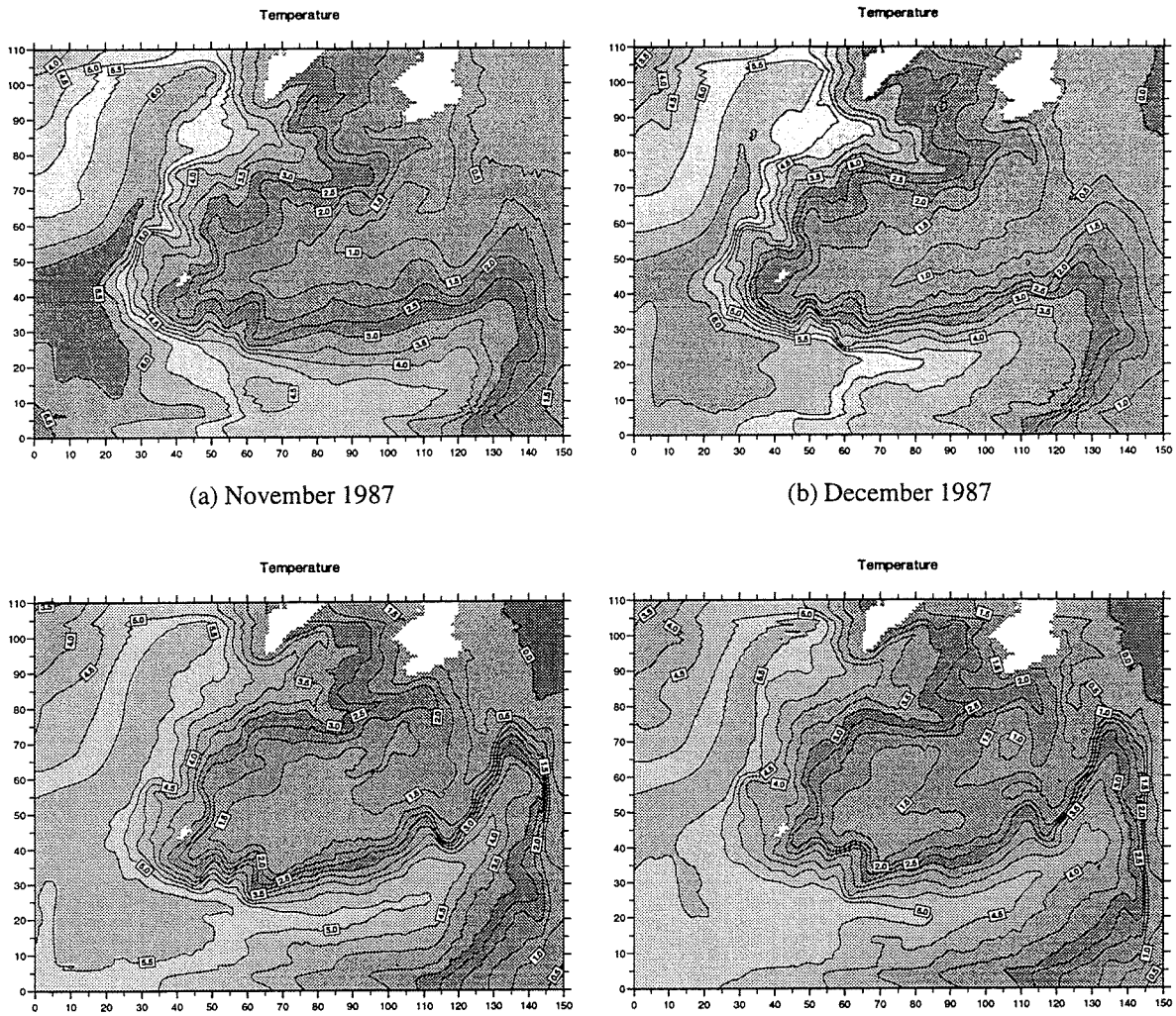

(a) November 1987

(b) December 1987

(c) January 1988

(d) February 1988

Figure 4.11: Modelled mean temperature at 10 m depth from the 4 km model.

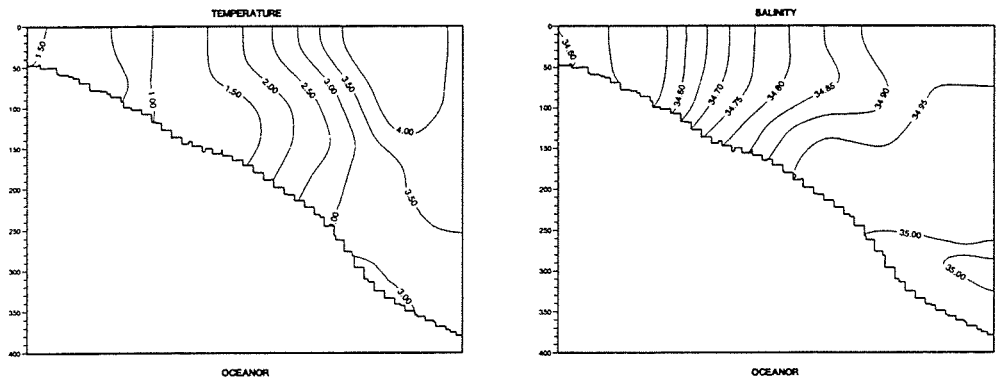

(a) December 1987 (b) December 1987

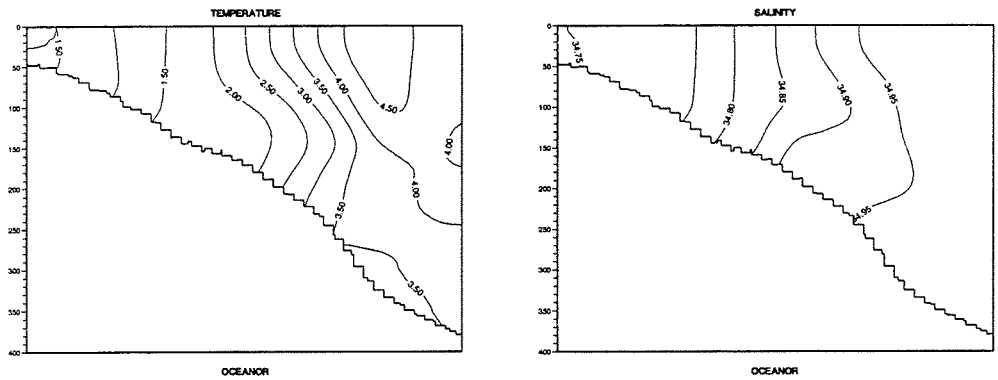

(c) February 1988 (d) February 1988

Figure 4.12: Modelled temperature and salinity at section Oceanor for two different months.

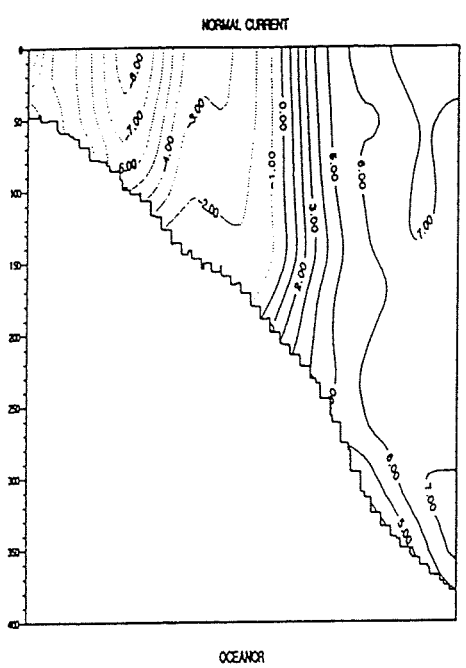

(a) Modelled current for November.

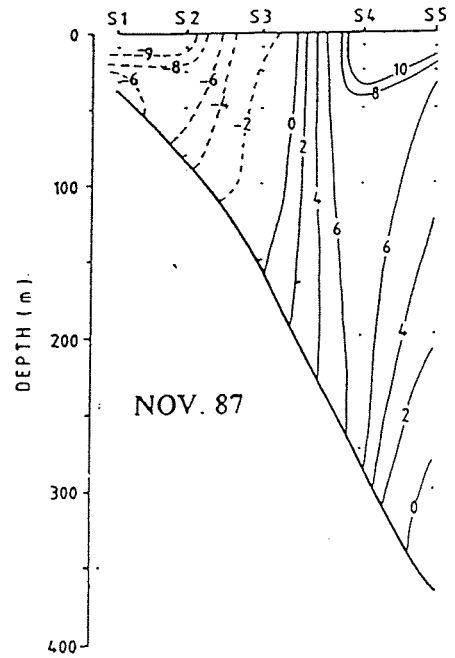

(b) Measured current for November.

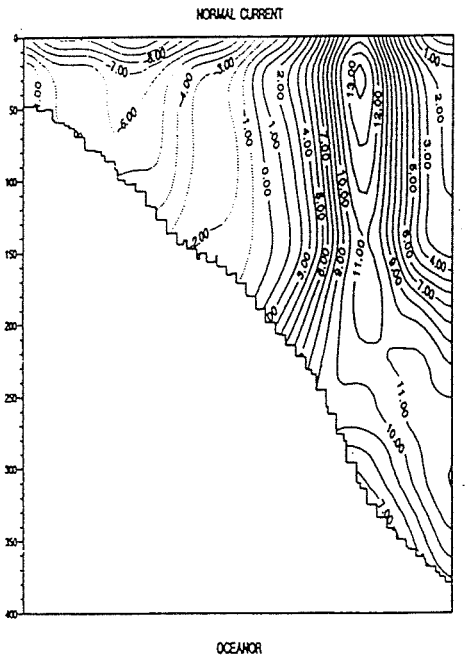

(c) Modelled current for December.

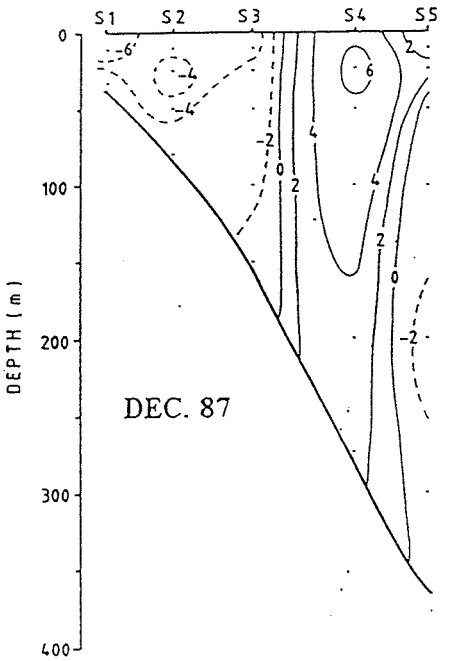

(d) Measured current for December.

Figure 4.13: Normal current along section Oceanor for the year of 1987. Left: Modelled. Right: Estimated from observations.

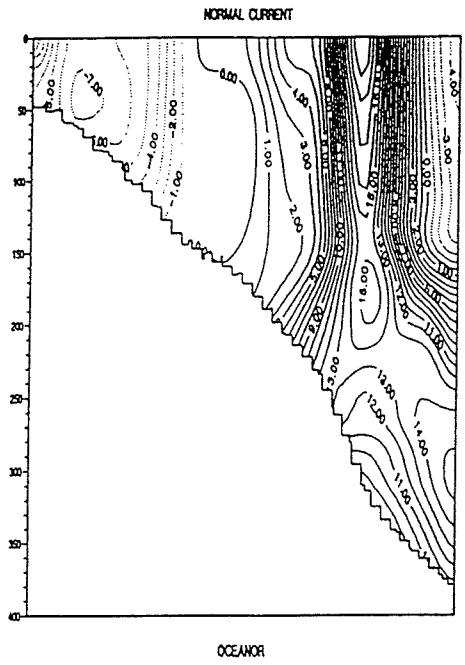

(a) Modelled current for January.

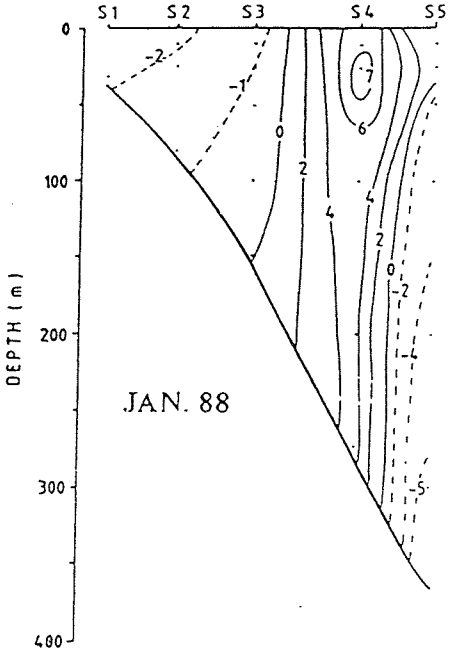

(b) Measured current for January.

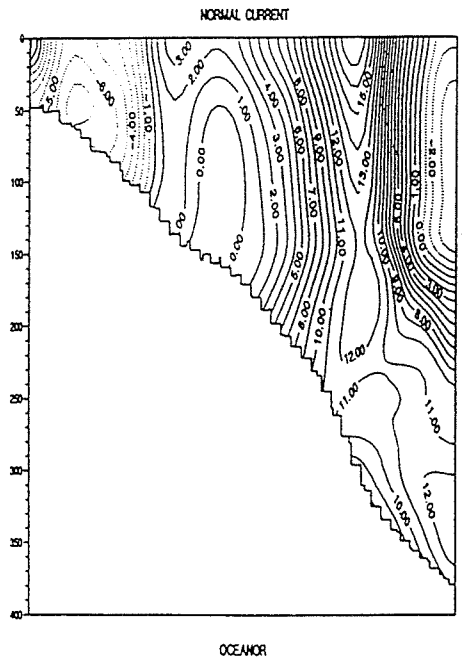

(c) Modelled current for February.

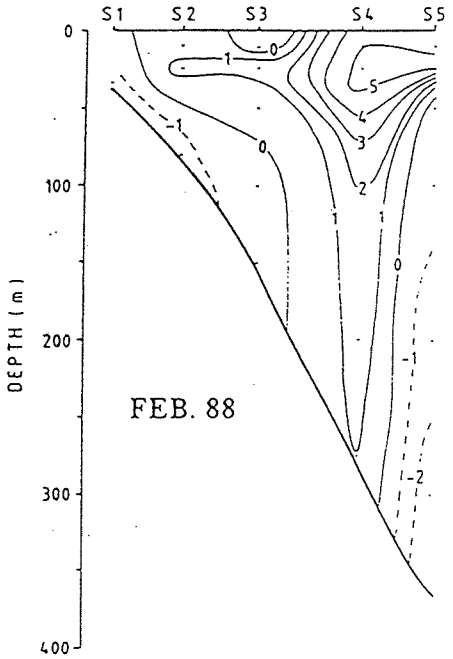

(d) Measured current for February.

Figure 4.14: Normal current along section Oceanor for the year of 1988. Left: Modelled. Right: Estimated from observations.

4.5 Discussion on the results from the hydrodynamic model

The summer hydrography on Svalbardbanken is quite complex. An overview is given in (Loeng, 1991). The observed sections agree with this general description. On top of the bank there is a well mixed layer, separated by a tidal front from a highly stratified ribbon with melt water at the surface and Arctic Water near bottom. Further out the Polar Front separates this ribbon from the Atlantic Water. The baroclinic Rossby radius of deformation in the area is in the order of 5 km.

The climatology mostly agrees with this picture. An exception is the Arctic Water which is not cold enough. This is probably due to the averaging processes performed while producing the climatology. The fields are somewhat smoother than the observations, as expected from a climatology. The observations from 1985 were used in the production of the climatology. As the data coverage in this area in 1985 is better than average, these observations have considerable influence on the climatology.

The modelled sections do not give the same impression. The Arctic and Atlantic water masses are placed correctly, but the melt water is not present or is to saline, the stratification is too weak and the water is not homogeneous on top of the bank. In other words, the quality of the salinity and temperature fields in the Svalbardbanken area deteriorate from the initial situation in July to the August mean.

These results clearly demonstrates that the mixing in the model is unrealistically high. This is a well known problem and is caused by artificial diffusion in the numerical methods and too poor vertical and horizontal resolution in the model.

The problem with the density structure is not easy to remedy without any freshwater sources in the model. The fresh surface water in the observations is caused by melting earlier in the season. For the time of the simulation Svalbardbanken is ice-free. Inclusion of a thermodynamic ice model would therefore not help with this simulation. In coastal areas fresh water outflow from rivers contribute to maintaining the salinity field, but this is not applicable here.

Using an artificial precipitation over the area might improve the result, but this has not been tested. Another alternative would be to use diagnostic simulations, that is, using the climatological hydrography instead of the model produced salinity and temperature.

As seen in the horizontal view, the Bear Island Current along the slope from North-East is rather week. The corresponding weak advection of fresh water may be part of the problem above. Vice versa, an improved stratification in the model, might lead to a stronger Bear Island Current. Too low transport of Arctic Water may also be caused by poor boundary description at the northern boundary of the 20 km model.

Several authors (Harms, 1992; Gjevik *et al.*, 1994; Kowalik & Proshutinsky, 1995) have pointed to the role of the tidal residual in shaping the Bear Island Current. Earlier sensitivity

experiments with the 20 km model alone gave similar results. It is therefore likely that inclusion of tides in the 4 km model would improve the Bear Island Current, and also help to create the summer tidal front.

During the winter, the conditions in the area is much more homogeneous and should therefore be easier to reproduce in a model. This seems to be true, the quality of the model results during winter is better than in the summer.

The qualitative the agreement with the current meters is very good. The Warm Core Jet and Bear Island Current are reproduced at the correct positions.

Quantitatively there are some problems, especially in January and February where the currents are too strong. One reason for this may be the lack of ice cover in the model, producing an erroneous stress on the sea surface. According to Li (1995) the Warm Core Jet is a barotropic current forced by the Norwegian Atlantic Current. The error in the current strength might therefore be caused by erroneous forcing at the boundary of the model domain.

5. DESCRIPTION OF THE TRANSPORT MODEL

At IMR a Lagrangian (particle based) transport model "LADIM" has been developed. The full documentation of this model will be given in (Ådlandsvik, 1997). This model has been used to simulate the transport of cod eggs and larvae (Ådlandsvik & Sundby, 1994) and herring larvae (Svendsen *et al.*, 1995).

5.1 Particle transport equations

The transport of a concentration ϕ in a current field is given by the advection-diffusion equation

$$\frac{\partial \phi}{\partial t} + \nabla \cdot (\mathbf{U}\phi) = \nabla \cdot (\underline{\mathbf{K}} \nabla \phi) \tag{5.1}$$

where $\mathbf{U}$ denotes the current vector and $\underline{\mathbf{K}}$ is the positive definite symmetric diffusivity tensor.

With a Lagrangian particle tracking method the concentration is modelled by a set of N "particles". The position of the i-th particle after the n-th time step is denoted $\mathbf{X}_i^n$. The set of all particles at a certain time step is called a *particle distribution* or a *particle cloud.*

To describe the time evolution of the particle distribution, the Euler Forward method is used for advection. Spatial variability in the current field leads to a spreading of the particles. In addition, diffusivity can be added by the *random walk* method. For the mathematical formulation a new vector field $\mathbf{A}$ and a new symmetric positive definite tensor field $\underline{\sigma}$ are used. They are defined by

$$\mathbf{A} = (\mathbf{U} + \nabla \cdot \underline{\mathbf{K}}) \tag{5.2}$$

$$\underline{\sigma} = \sqrt{2\underline{\mathbf{K}}} \tag{5.3}$$

The displacement of a particle during one time step is then given by

$$\mathbf{X}_i^{n+1} - \mathbf{X}_i^n = \mathbf{A}_i^n \Delta t + \underline{\sigma}_i^n \mathbf{Q}_i^n \sqrt{\Delta t}. \tag{5.4}$$

Here $\mathbf{Q}_i^n$ is a normalised random (or stochastic) vector whose components are independent with zero mean and unit variance. In other words, $E(\mathbf{Q}) = \mathbf{0}$ and $E(\mathbf{Q}\mathbf{Q}^T) = \underline{\mathbf{I}}$, the identity tensor, where E is the expected value operator. The $\mathbf{Q}_i^n$-s for different i and/or n are also independent.

Without the divergence term in (5.2) the random walk method produces an erroneous concentration effect in areas of low diffusivity. The correspondence between (5.4) and (5.1) can be established by the theory of stochastic differential equations. Alternatively, it can be explained by comparing the time development of the moments of the distribution. This approach is used by Ådlandsvik (1997).

With no diffusion, $\underline{\underline{K}} = \underline{\underline{0}}$, this reduces to the Euler Forward method for solving an uncoupled system of ordinary differential equations. More advanced methods exist for this purpose, but with the uncertainties in the current field, the extra effort is not necessary.

5.2 Set-up of the transport model

This section describes the settings used to apply LADIM to the study of transport of eggs and larvae of polar cod. The eggs of polar cod are pelagic and is expected to be found close to the surface under the ice. For the larvae, not much is known about their vertical behaviour.

In the model, the particles are confined to a fixed depth, usually 10 m. The horizontal current fields are taken from the simulations in chapter 4, in particular the winter 1988 simulations.

The horizontal mixing is taken homogeneous and isotropic with a value of $100\,\mathrm{m^2 s^{-1}}$. This is the same value as used in (Ådlandsvik & Sundby, 1994). With a time step of 30 minutes, this correspond to a random kick of the particles with axisymmetric distribution with standard deviation 600 m by equation (5.4).

6. RESULTS FROM THE TRANSPORT MODEL

6.1 A standard run

For simulations of the larvae distributions, the year 1988 was chosen. part of the motivation for this choice is that the period is partly covered by the Oceanor current meters (sections 3.3 and 4.4).

The 0-group distribution of Polar Cod in 1988 is depicted in figure 1.1 taken from (Gjøsæter & Anthonypillai, 1995). The 1988 distribution is not untypical. The high concentrations west of Spitzbergen occurs in almost all years. The distribution extends somewhat further to the south and east than average, without being extreme in this respect.

6.1.1 Meteorological conditions

The only driving force for the model that is specific for 1988 is the meteorological forcing. To interpret the results from the 1988 particle tracking simulations, an overview of the wind conditions is useful. Figure 6.1 shows the monthly mean wind fields for the Barents region. These results are produced by averaging the 6-hourly wind fields from DNMI's Hindcast Archive (section 3.2).

The wind pattern is variable throughout the period. On Svalbardbanken easterly winds (winds *from* east) dominate. The month June is an exception with quite strong westerly winds. East of Svalbard the most common wind direction is northerly, but during February, June and in particular August the wind direction is southerly in this area.

In addition to the POM model, IMR have a simpler purely wind-driven barotropic model for the Barents Sea (Ådlandsvik, 1989). This model has been used to make a time series of the wind-driven inflow to the Barents Sea (Ådlandsvik & Loeng, 1991; Loeng *et al.*, 1995). Figure 6.2 compares the model inflow for 1988 to the mean. In January and even more in February the inflow is lower than normal, approximately one standard deviation. During March and April the inflow was a little higher than the mean. For May and June the inflow is very close to the mean and thereafter decreases in July and August. Overall, the model inflow series from 1988 does not suggest any extreme atmospheric forcing that would make 1988 unusable as a standard year in these investigations.

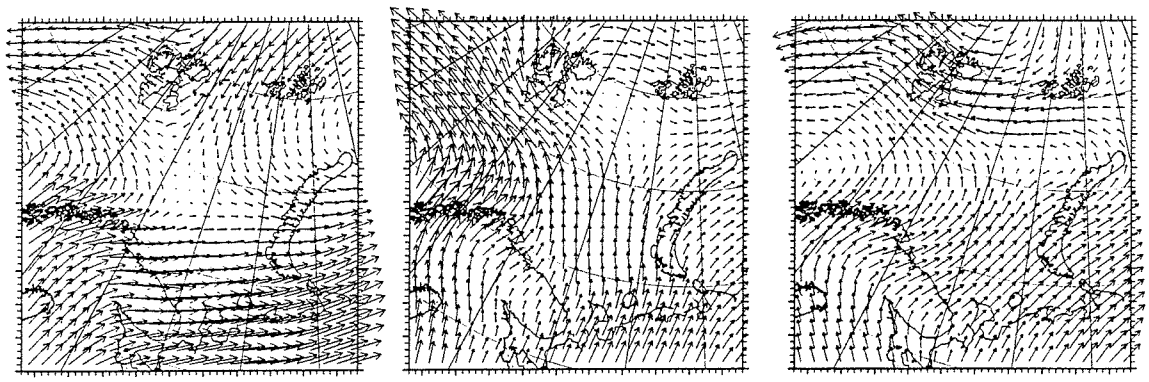

(a) January (b) February (c) March

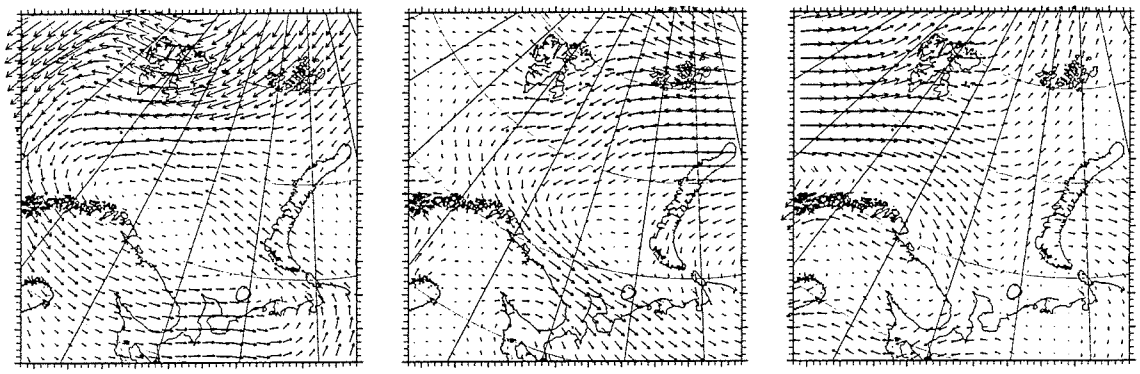

(d) April (e) May (f) June

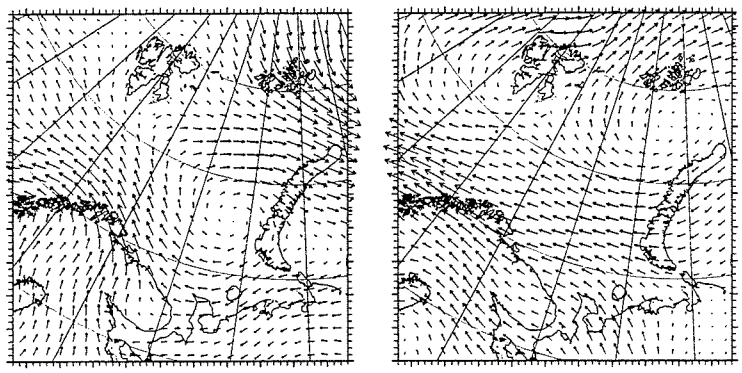

(g) July (h) August

Figure 6.1: Monthly mean wind fields from January to August 1988

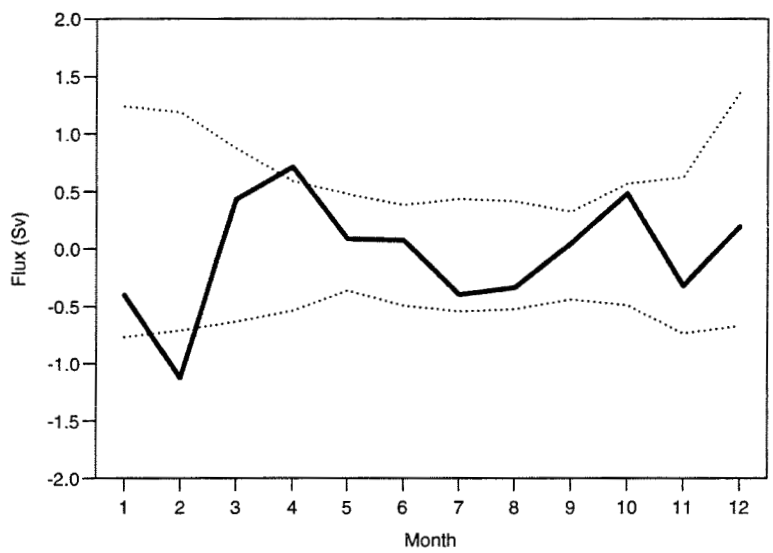

Figure 6.2: Monthly mean modelled wind-driven volume flux through the Fugløya–Bjørnøya section in 1988. The dotted lines are the mean for the period 1970–1994 plus/minus one standard deviation

6.1.2 Current conditions

Figure 6.3 shows the monthly averaged horizontal current fields from the 4 km model. The depth is 10 m. For the first months a vertical section of the current field is compared to the array of current meters described in section 3.3.

The most persistent feature is the strong Atlantic Current in west following the shelf edge and continuing as the West Spitzbergen Current. Another persistent current is the Warm Core Jet outside the 200 m isobath south of Svalbardbanken with direction towards east and north. The strength of this current varies and it is particular strong in February, June, and July. Further up on the slope of the bank, there is a weaker Bear Island Current in the opposite direction towards Bjørnøya. In some months, March in particular, this current is hardly recognisable. Compared to the standard view of the Barents Sea circulation (fig. 1.2) this current is too weak.

On Svalbardbanken the current is generally weak and varying and the model produces some eddy activity in the area. The main flow direction in towards north to north west. An exception here is June with southwards flow. This is consistent with the reversed wind field that month. The exception in June may be part of the explanation of the southern and eastern extent of the 0-group distribution of polar cod in 1988.

South of Svalbard the model produces occasionally strong currents. The direction is variable, towards east in January, February, and June, and westerly in March and April. East of Edgeøya the current is generally weak and variable. During February and to less degree March this area has a considerable northerly flow.

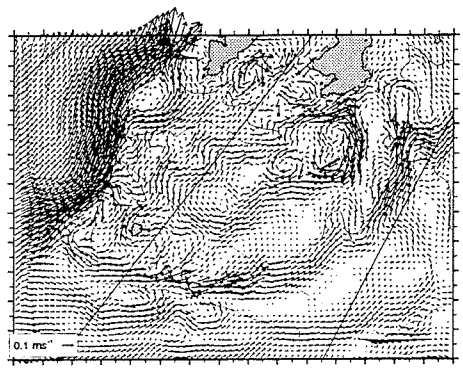

(a) January

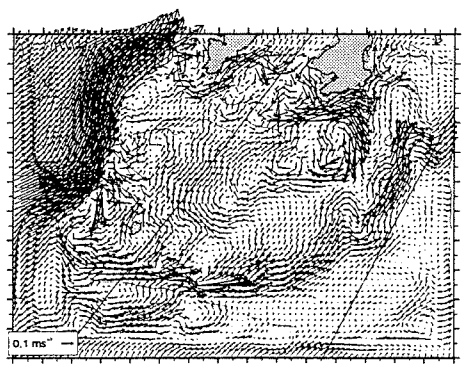

(b) February

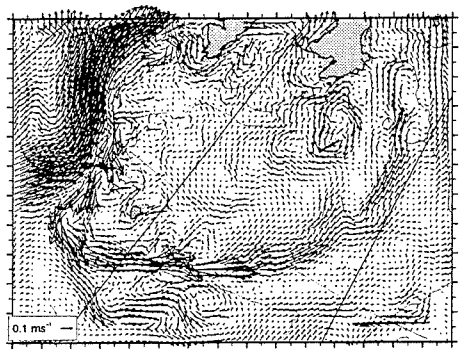

(c) March

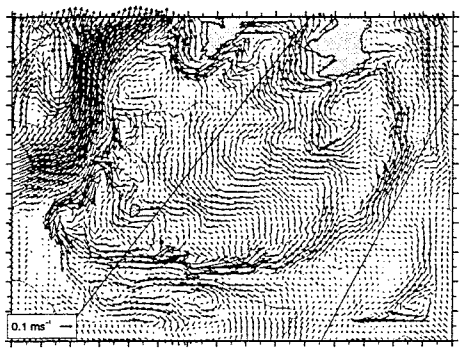

(d) April

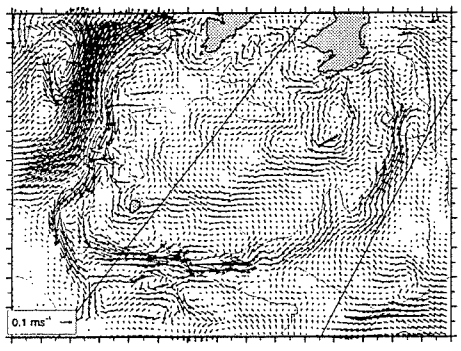

(e) May

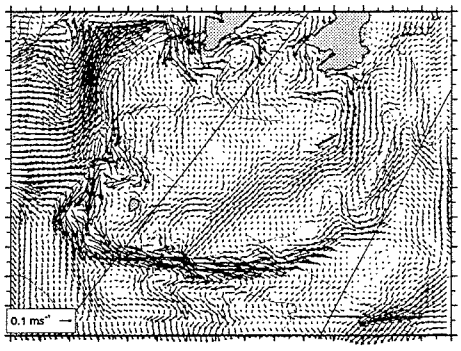

(f) June

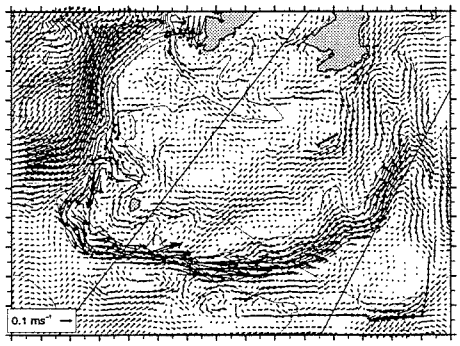

(g) July

Figure 6.3: Monthly averaged modelled current fields in 10 m

6.1.3 Particle transport

For the standard run of the transport model, the particles were released in a position close to 77°N and 25°E between Edgeøya and Hopen, at 1 January 1988. This date may be to early as a spawning date, but were chosen to illustrate the particle transport for the whole simulation period. A total of 1000 particles were released and the transport depth were fixed at 10 m. The particle distributions at the beginning of each month are given in fig. 6.4. Table 6.1 summarises some statistics of the particle distributions, the number N of particles remaining in the area, the longitude λ and the latitude ϕ of the mass centre $\overline{\mathbf{X}}$ of the particles and the radial variance σ^2 of the distribution. The later is defined as

$$\sigma^2 = \frac{1}{N-1} \sum_i \|\mathbf{X_i} - \overline{\mathbf{X}}\|^2. \tag{6.1}$$

Sim. time	Date	N	λ	ϕ	σ^2
0	1 January	1000	25.16	77.11	0.0
31	1 February	980	25.84	76.79	527.8
60	1 March	748	26.10	77.00	814.8
91	1 April	430	23.58	77.04	741.7
121	1 May	252	19.31	76.70	607.0
152	1 June	183	18.24	76.46	909.1
182	1 July	161	20.45	75.89	876.3
213	1 August	158	20.57	75.84	849.7

Table 6.1: Particle statistics for the standard run

During the simulation period 84% of the particles are lost. The main part of the loss is due to northeast transport out of the area east of Edgeøya, primarily in March and April. This is consistent with the current fields in fig 6.3 where the average for these months have a component out of the model domain. After this period there area east of Edgeøya is almost depleted for particles. Later in the period some particles are also lost from the 4 km domain into Storfjorden.

Figure 6.5 presents the distributions from the standard run after 50, 100, 150 and 200 days. These day numbers will be used later for comparison with other simulations. In figure 6.6 the particle positions are shown in the 20 km domain where the results from the 20 km run of the current model are used outside the 4 km domain. These distributions confirm that the particles are lost towards north east of Edgeøya.

The remaining particles went onto Svalbardbanken in March and were transported northwards in April and May. In June, the wind direction changed to westerly (fig. 6.1). This induced

a southwards currents on the bank, where the particles are spreading out over the bank again. In July the wind was rather weak and the remaining particles became spread out over a larger area.

Only a few particles are transported southwest to Bjørnøya and very few of them are caught by the Atlantic Current towards West Spitzbergen.

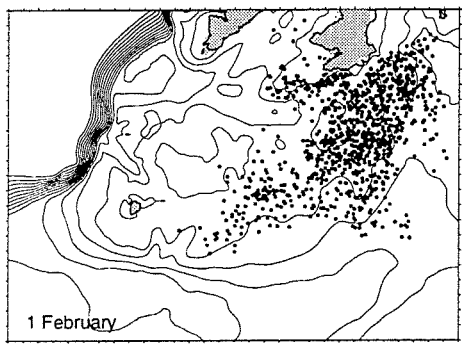

(a) 1 February

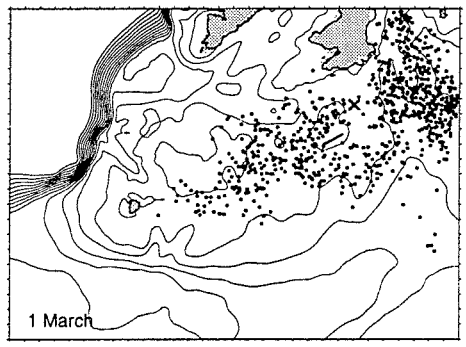

(b) 1 March

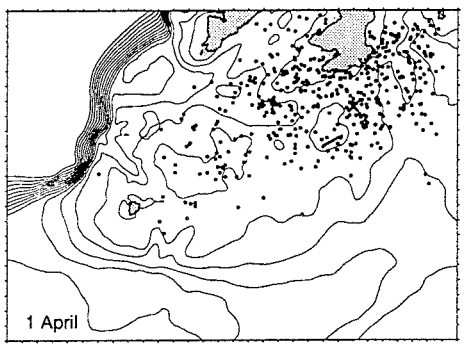

(c) 1 April

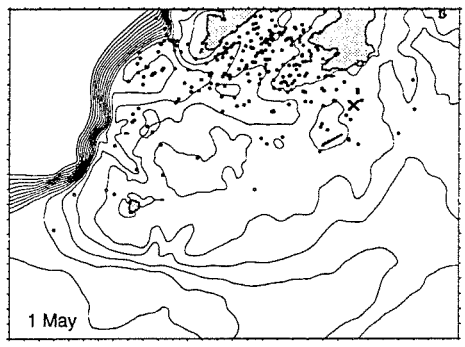

(d) 1 May

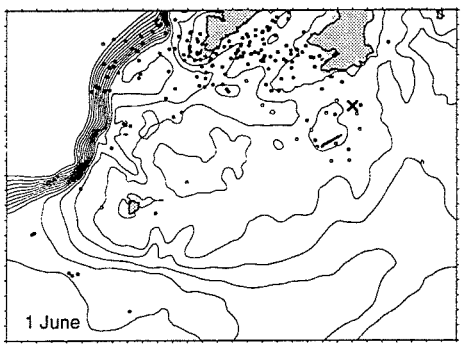

(e) 1 June

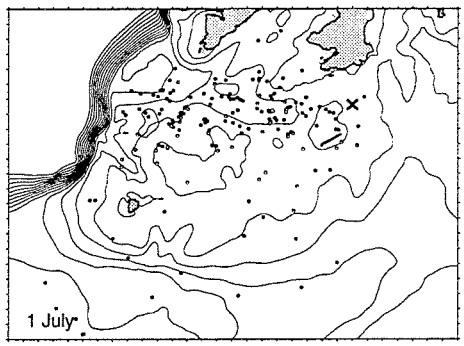

(f) 1 July

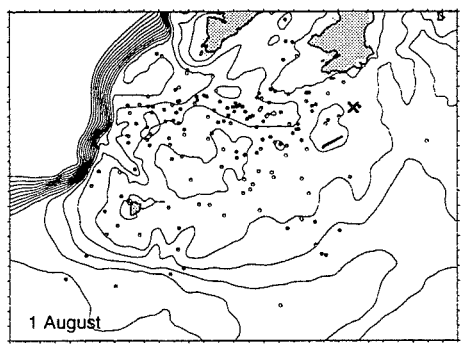

(g) 1 August

Figure 6.4: Particle distributions from first day of each month

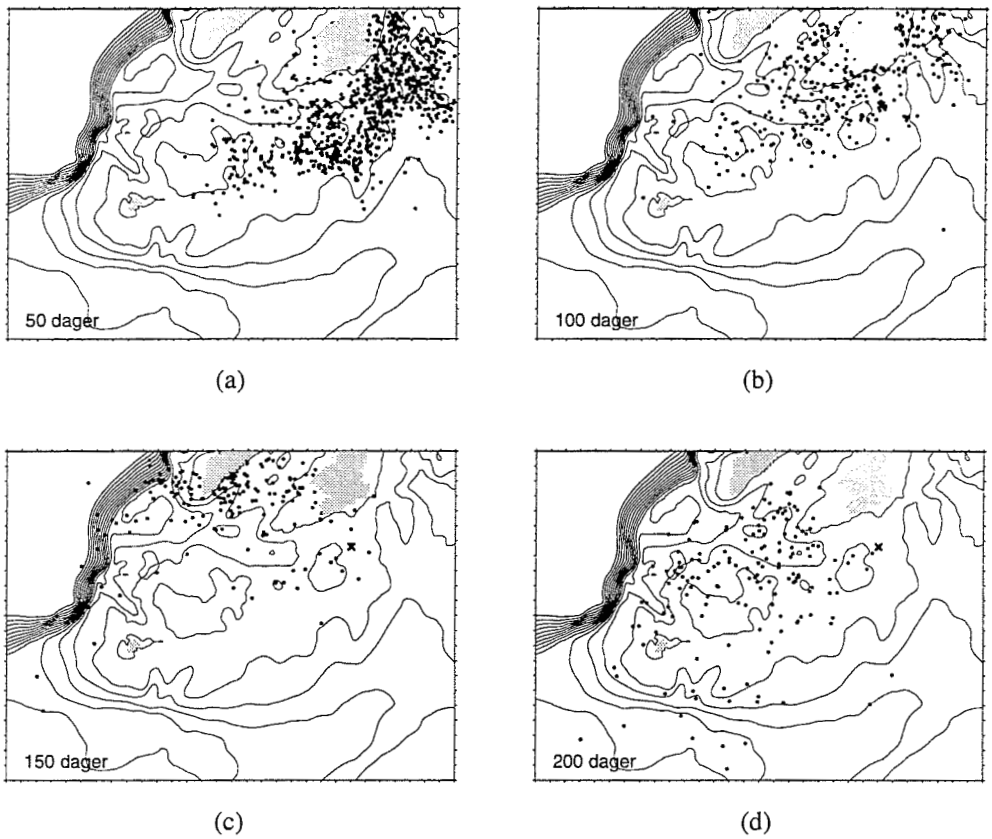

Figure 6.5: Particle positions from the standard run of the transport model

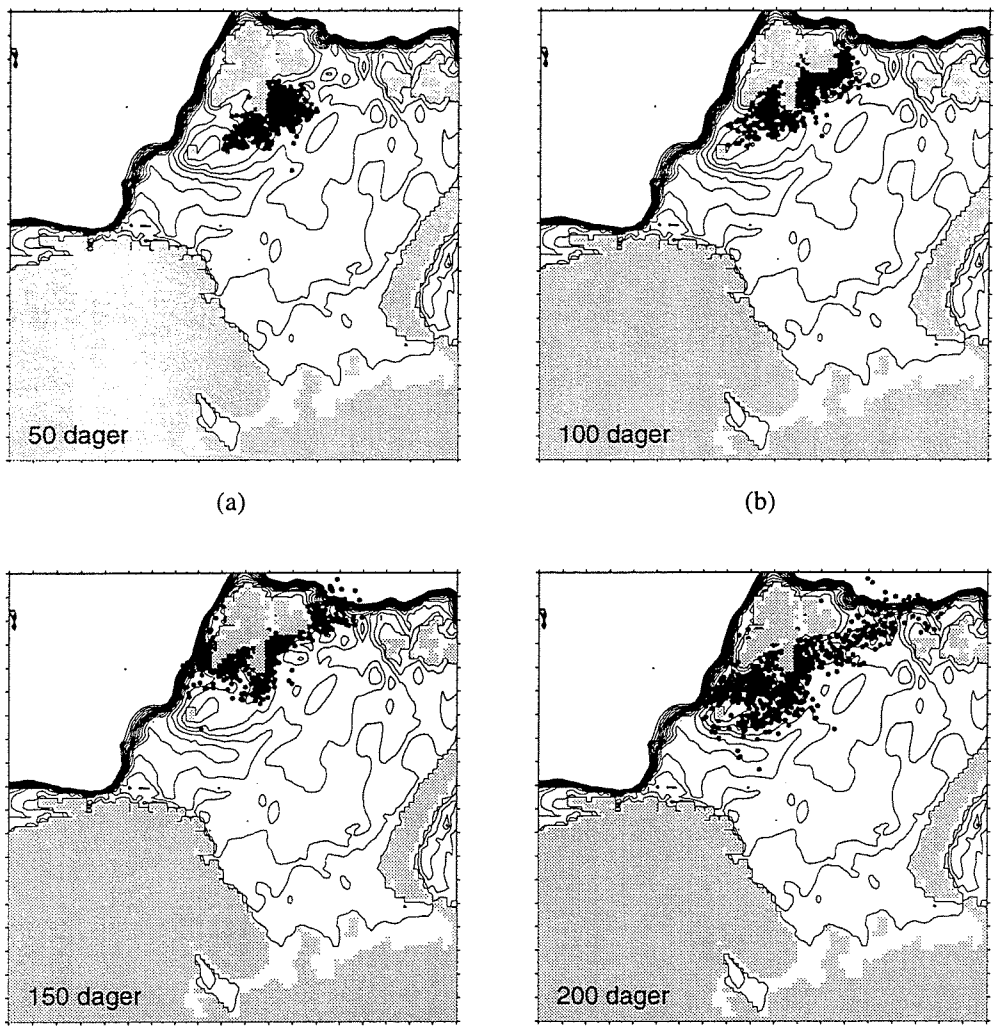

(a) (b)

(c) (d)

Figure 6.6: The positions of the particles after 50, 100, 150 and 200 days in the 20 km model. Particle release point is (77° N, 25° E) at depth 10 m. Start 1 January 1988.

6.2 Sensitivity studies

To properly interpret the results from the transport model, it is necessary to have some knowledge of how changes in the forcing and parametrisation influences the model results. In this section the sensitivity to transport depth and simulation period will be examined.

6.2.1 Transport depth

The trajectories do not differ very much form the standard run when depths of 5 or 20 m are used. It is not easy to decide if this is a real feature or an artifact of missing vertical resolution in the hydrodynamical model. Going further down to 50 m the results are quite different from the near-surface transport. The 50 m results are shown in figure 6.7.

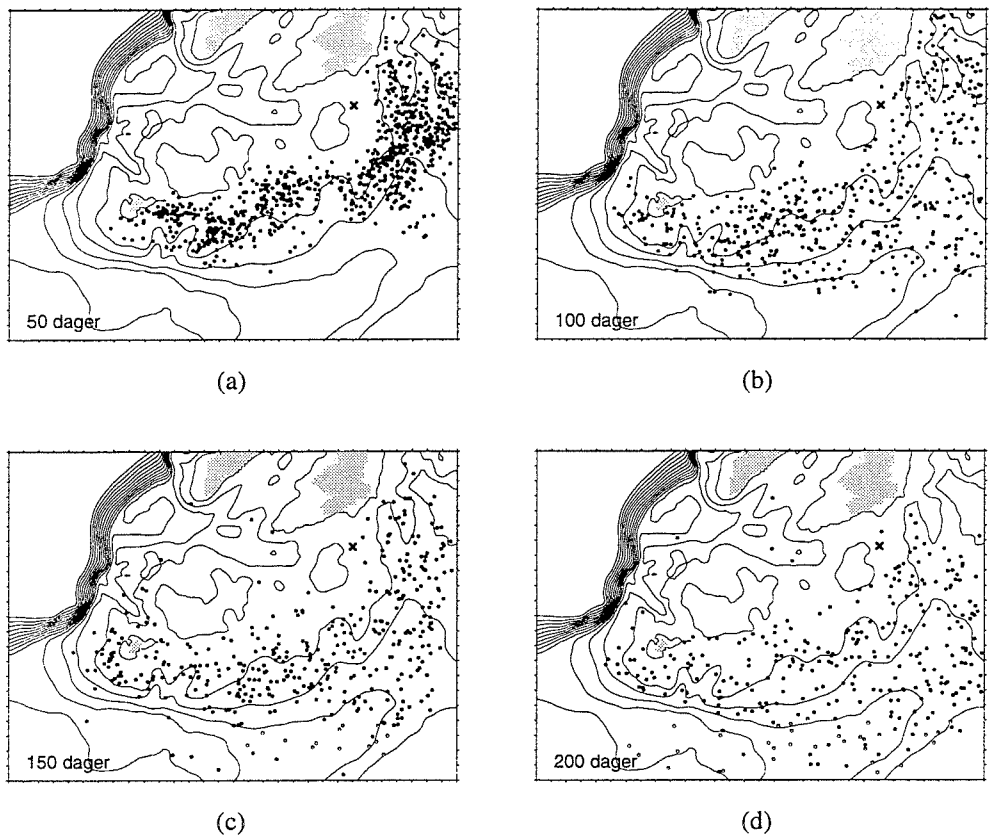

Figure 6.7: The positions of the particles after 50, 100, 150 and 200 days in the 4 km model. Particle release point is 77°N, 25°E at depth 50m. Start 1 January 1988.

As large parts of Svalbardbanken is shallower than 50 m the bank act as a barrier for the particles. As a result, the particles are distributed along the southern slope of the bank, from

Bjørnøya towards northeast. As time goes on, the particles are spread by the diffusion. Very few of the particles gets into the northwards current west of Bjørnøya.

6.2.2 Simulation period

To test the dependence on the simulation period, similar runs to the standard run were performed with the particles released at 1 February and 1 March. The results are presented in fig. 6.8 and table 6.2 for the 1 February run and fig. 6.9 and table 6.3 for the 1 March run.

Sim. time	Date	N	λ	ϕ	σ^2
0	1 February	1000	25.16	77.11	.0
29	1 March	991	26.47	76.82	425.1
60	1 April	740	24.39	77.12	491.9
90	1 May	491	19.86	76.86	420.1
121	1 June	347	18.66	76.71	595.2
151	1 July	307	20.85	76.15	608.4
182	1 August	304	20.83	75.99	669.6

Table 6.2: Particle statistics for the run starting 1 February

Sim. time	Date	N	λ	ϕ	σ^2
0	1 March	1000	25.16	75.11	0.0
31	1 April	996	25.21	76.83	242.3
61	1 May	857	20.24	76.90	311.8
92	1 June	651	18.84	76.74	524.3
122	1 July	590	20.88	76.15	541.4
153	1 August	584	20.85	76.04	647.6

Table 6.3: Particle statistics for the run 1 March

The general impression, both from the figures and the tables, is that the particle distributions are very similar. In all cases the particles are spread out over Svalbardbanken and Storfjordrenna. The centres of mass are almost identical. The main difference is the number of particles left in the area.

Looking closer at the time evolution, it is clear that they are shapened by the same current history. For instance all particles are transported westwards in April and south in June. A period of 2–3 months is needed before the younger particles catch up with the older.

For the 1 January run, most of the particles disappeared in March and April towards north east of Edgeya. At this time the younger particles had not yet reached this area and were to little or no degree affected by that event.

For comparison, a completely different simulation period was chosen using the summer current field from the summer 1985. This period were also used in the validation studies in section 4.3. Using the same release point, 1000 particles were released on 1 July. Figure 6.10 show the particle distributions after 50, 100 and 150 days. In this case the particles are initially spreading south and west and cover the bank after 100 days. After 150 days the particles have left Svalbardbanken towards north and are concentrated from Storfjordrenna and eastwards.

These particles are transported south and east during the first 50 days, thereafter west again and spreading out over Svalbardbanken. In the last 50 day period the particles are moved north. This is quite different from the winter 1988 simulations.

For this area it seems that the precise "spawning time" is not important for transport times of 3 months ore more in this area. As the model current is not particularly strong and stable, the integrated histories of winds and currents give more or less the same result. In a region dominated by strong advection this would not happen, as the youngest particles would never be able to catch up with the older. This argument can be turned around. In this form, it indicates that it is not possible to pinpoint the spawning time from observed 0-group distribution and knowledge of the current history.

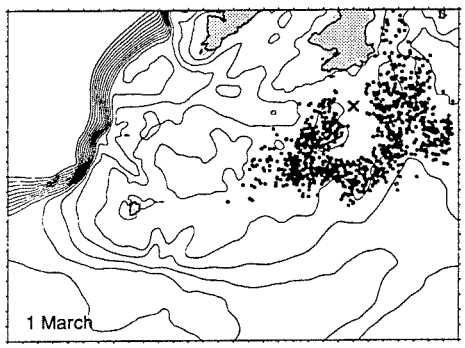

(a) 1 March

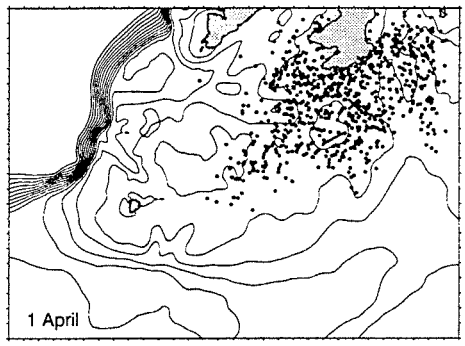

(b) 1 April

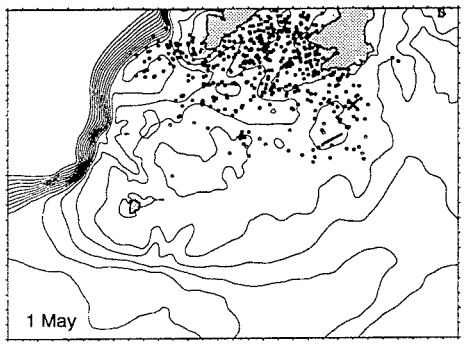

(c) 1 May

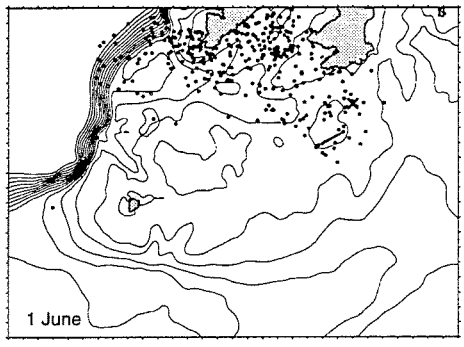

(d) 1 June

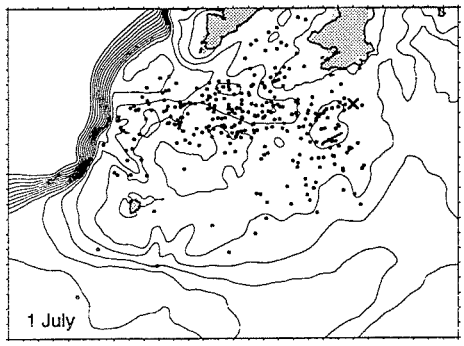

(e) 1 July

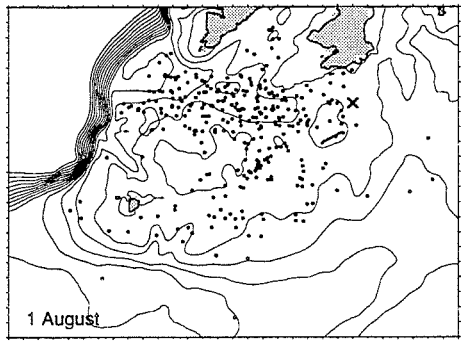

(f) 1 August

Figure 6.8: Particle distributions from first day of each month. Simulation started 1 February 1988.

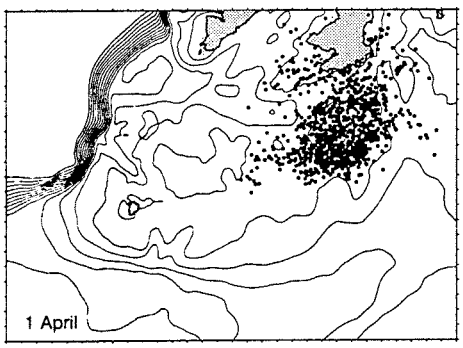

(a) 1 April

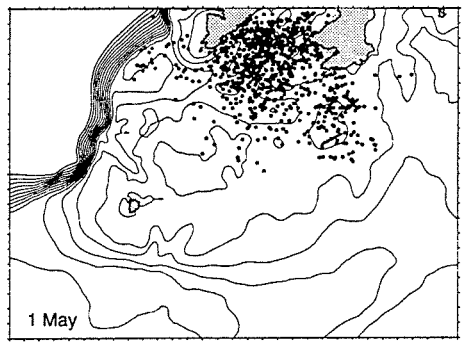

(b) 1 May

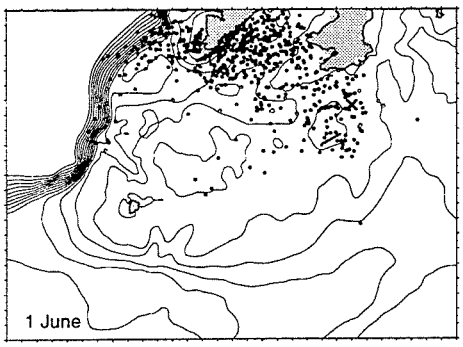

(c) 1 June

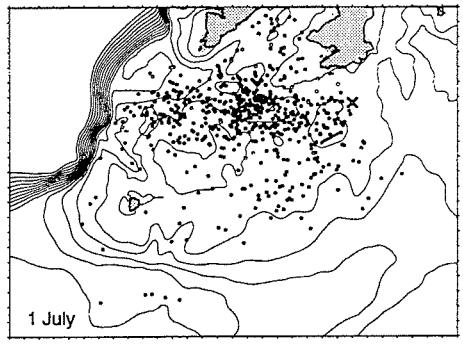

(d) 1 July

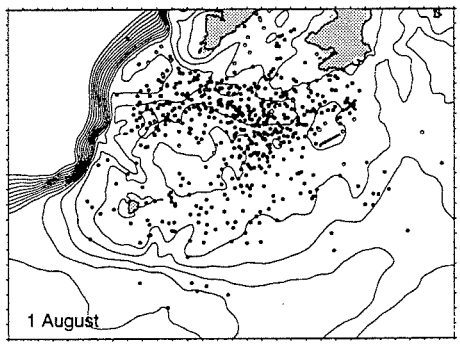

(e) 1 August

Figure 6.9: Particle distributions from first day of each month with particles released 1 March.

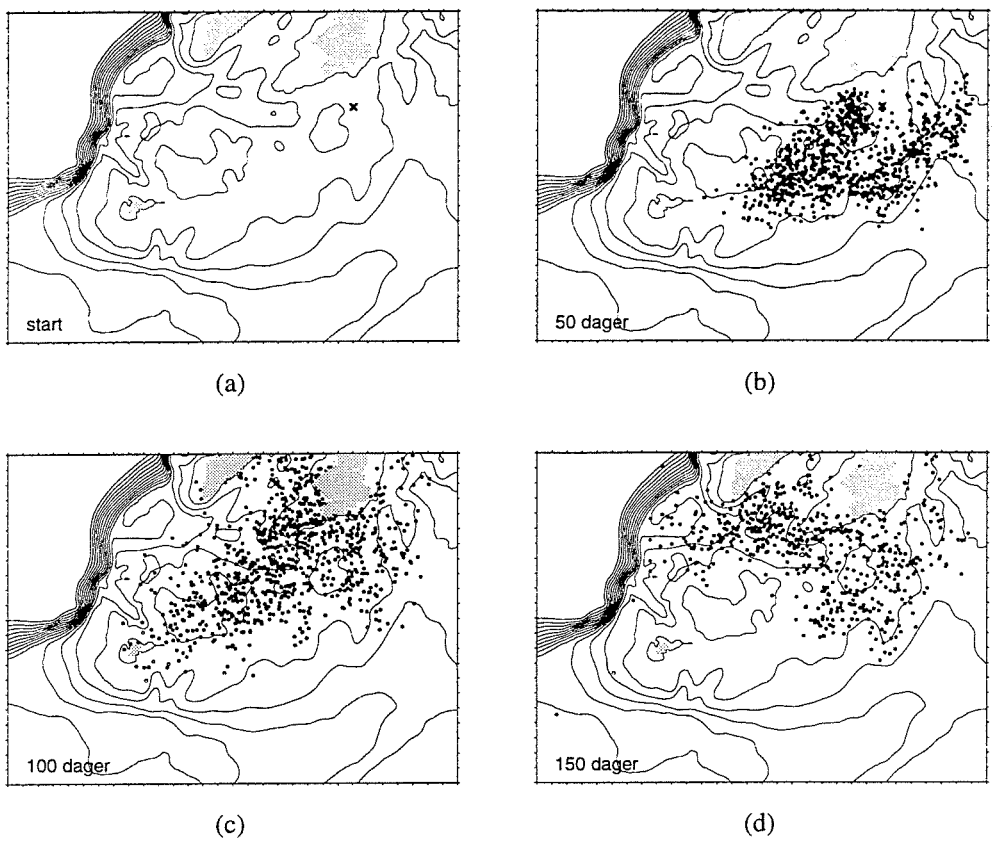

Figure 6.10: The positions of the particles after 0, 50, 100 and 150 days in the 4 km model. Particle release point is (77° N, 25° E) at depth 10 m. Start 1 July 1985.

6.2.3 Release position

To test the dependence on the start position an array of 3 by 3 points surrounding the "standard point" was chosen. The distance between the points is 10 grid-cells (i.e. 40 km). In addition 6 points further south and west on the Bank were used. The positions are marked with an "×" in figure 6.11. The figure also contain the the particle trajectories starting in the points at 1 February and drifting until 1 August. This simulation is done without random walk diffusion.

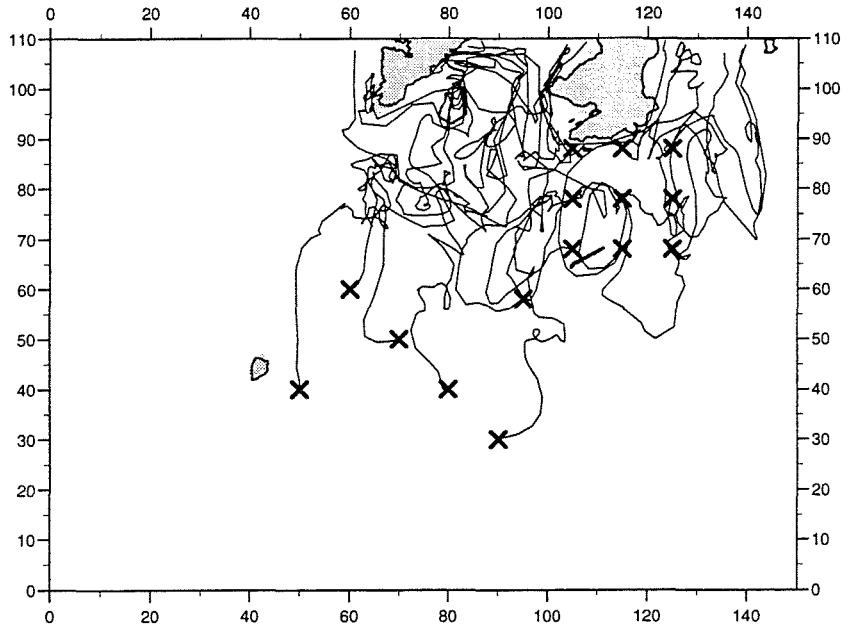

Figure 6.11: Particle trajectories without diffusion from selected start points

A set of model runs were performed, releasing 1000 particles in each of the 15 points at 1 February and running until 1 August. Table 6.4 gives the grid-coordinates x, y of the start point, the number N of particles remaining in the area at 1 August, their centre of gravity with longitude λ and latitude ϕ and their radial variance σ^2.

Nearly all particles starting in the right column were lost. Also the upper positions gave very high loss rate. Except for the right column the centre of gravity and spreading of the distributions are very similar.

Figure 6.12 shows the resulting particle distributions at 1 August from the 8 surrounding points. The corresponding result from the standard position (115, 78) is shown in fig. 6.4(f). The distributions with more than 100 particles remaining are very similar.

In view of the results with different spawning time this is not surprising. The particles "flushes around" in the same area and are influenced by more or less the same wind and current events. For polar cod, it indicates that the 0-group distribution does not depend to much

x	y	N	λ	ϕ	σ^2
115	78	304	20.57	75.99	669.6
105	68	317	20.90	76.01	622.2
115	68	237	20.78	75.99	624.4
125	68	21	22.00	72.91	988.9
125	78	21	22.26	76.15	783.0
125	88	4	21.36	76.14	335.5
115	88	89	20.91	76.17	661.4
105	88	81	20.99	76.08	766.4
105	78	197	20.53	75.93	651.2
95	58	350	20.43	75.91	769.8
50	40	232	20.15	75.30	1179.9
60	60	168	20.31	75.74	950.3
70	50	185	20.33	75.75	888.3
80	40	464	20.10	75.62	959.2
90	30	646	20.42	75.88	695.3

Table 6.4: Particle statistics for 1 August with different start positions

on the precise spawning area. Or reversed, that the spawning area is difficult to determine from knowledge on 0-group distribution and current conditions.

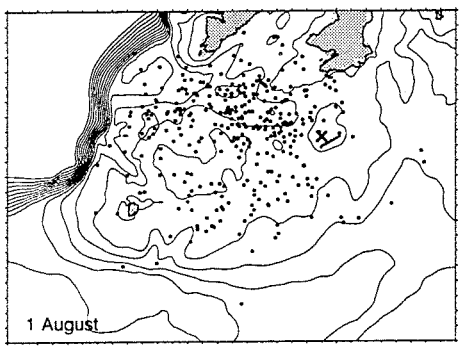

(a) 105, 68

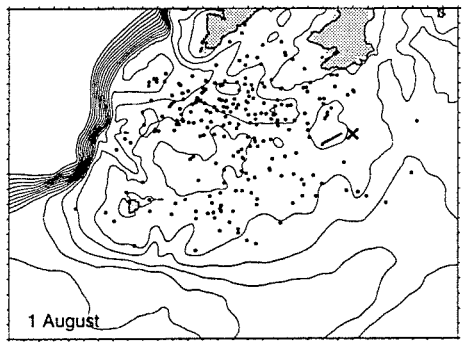

(b) 115, 68

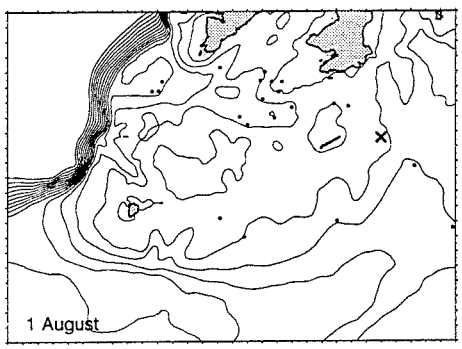

(c) 125, 68

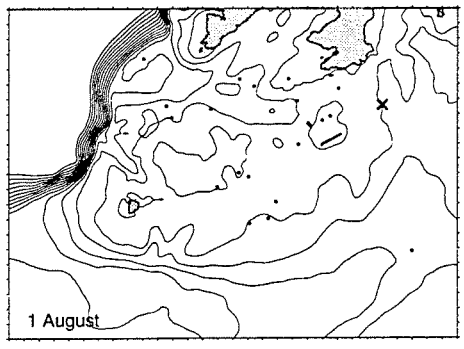

(d) 125, 78

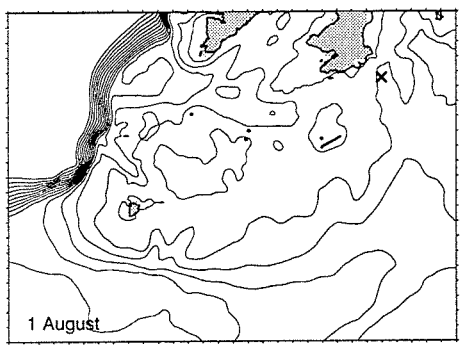

(e) 125, 88

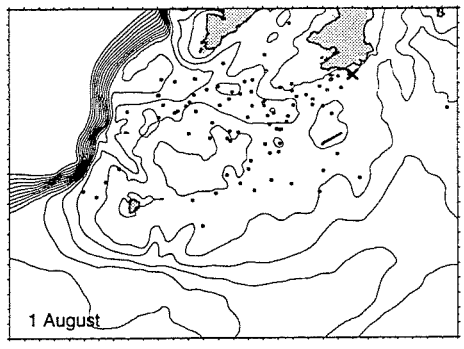

(f) 115, 88

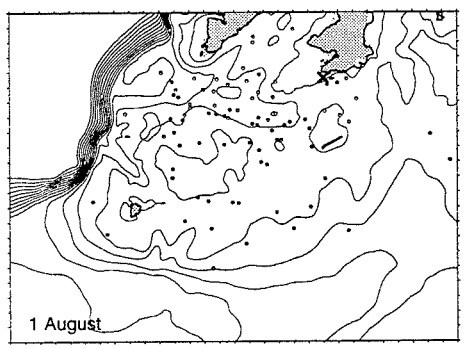

(g) 105, 88

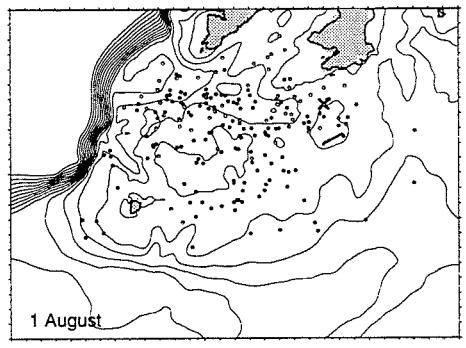

(h) 105, 78

Figure 6.12: Particle distributions at 1 August with different start positions

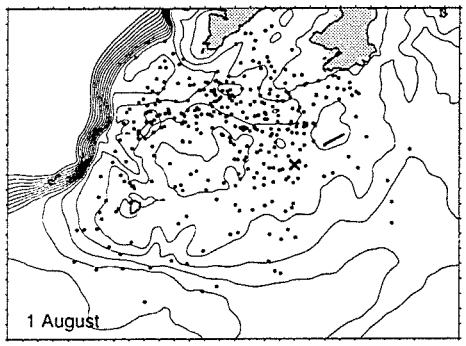

(a) 95, 58

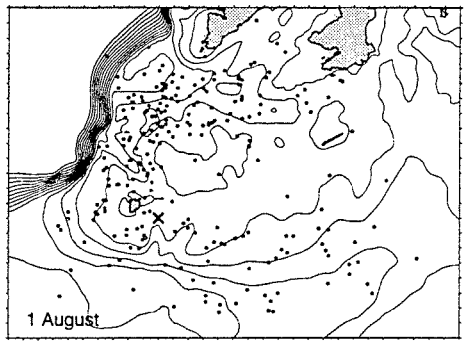

(b) 50, 40

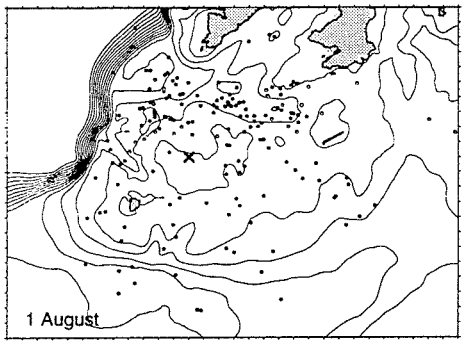

(c) 60, 60

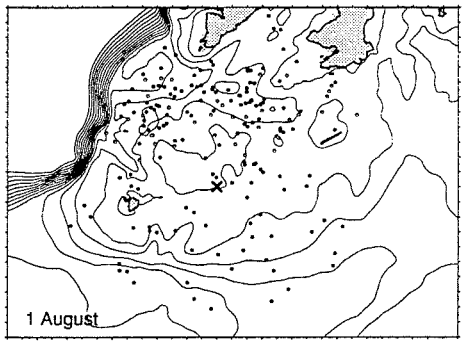

(d) 70, 50

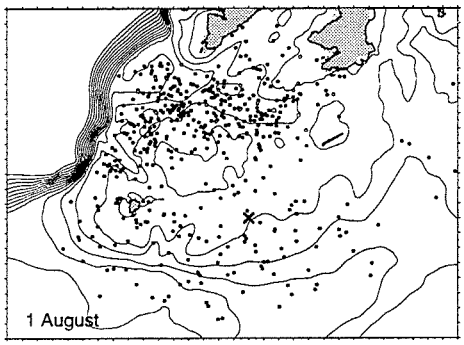

(e) 80, 40

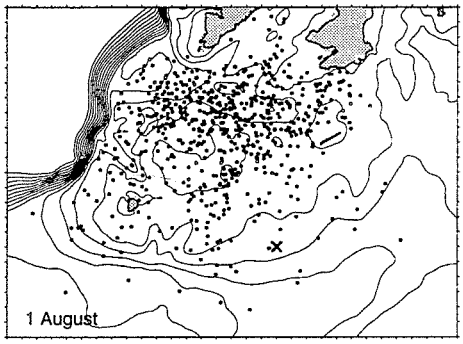

(f) 90, 30

Figure 6.13: Particle distributions at 1 August with marked start positions

6.3 Backwards trajectories

The LADIM particle tracking model can also be used to track trajectories backwards in time. In this case the random walk diffusion, which is an irreversible process, must be turned off. By using this feature, it is in principle possible to follow model trajectories leading up to the positions with high density of early juvenile polar cod.

Backwards trajectories from nearby points will be dispersed by current shear in the same same way as forward trajectories. For long time periods backwards, a handful of backwards trajectories will therefore be critically dependent on the "initial" (really final) position.

In the early juvenile distribution from 1988 in figure 1.1 there are two areas in the west with higher concentration. The first is south of Spitzbergen at about 76°N and the other is on the narrow shelf west of Spitzbergen. The latter is also interesting, because the forward simulations gave almost none particles in this area.

Backwards trajectories from these areas are given in fig 6.14. The final positions are indicated by "×". The trajectories extends 30 days backwards from the 1 July 1988.

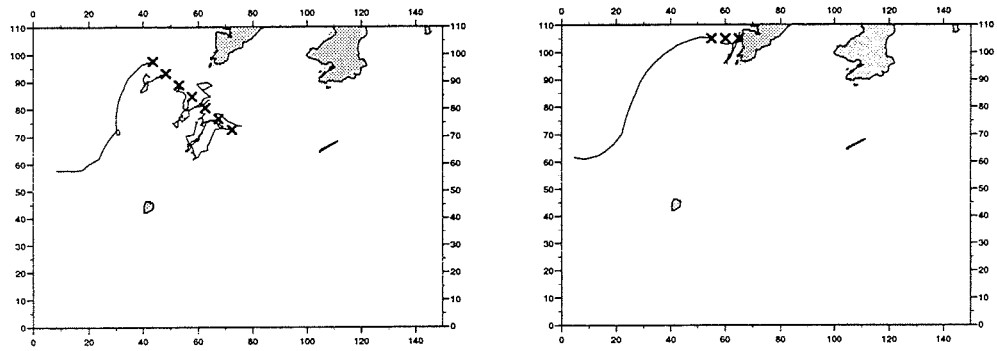

(a) (b)

Figure 6.14: 30 days backwards trajectories from 1 July 1988.

The positions in sub-figure (a) have latitude 76°N. The western-most particle is coming with the Atlantic Current at the shelf edge. The other trajectories are less stable but indicate a slow drift south. This is consistent with the modelled current picture for May , figure 6.3(e). With the model current field, particles in these positions (except the western-most) can very well come from areas around Edgeøya and Hopen.

Some positions west of Spitzbergen are considered in figure 6.14(b). Here too, the western-most particle is coming with the shelf edge current. The other particles on the narrow shelf are moved a little back and forth with the weak and variable current. With the current description

provided from the model, it is not likely that many particles from south of Edgeya will reach this area. Instead, the particles tend to be remain on the narrow shelf.

7. CONCLUDING REMARKS

The main novel feature of this work is that a nested version of a 3D baroclinic model has been set up and evaluated for the northwestern Barents Sea. To the best of our knowledge, this has not been done before. The objective of the model was to produce a realistic current picture in the area. Qualitatively at least, this was fulfilled in that the currents were reproduced at the correct locations. The quality of the results from the hydrodynamical model were discussed further in section 4.5.

There is a clear potential for improvement of the model results. This can be done by incorporating more physics, in particular tides and sea ice. The resolution, both horizontally and vertically, is also limiting for the quality of the results. Another important factor is the input data to the model, in particular the initial and boundary description of hydrography and currents for the 20 km model.

The distribution of early juvenile polar cod is determined by the physical transport, the growth and in particular the survival of the earlier stages. The particle tracking model only considers the transport processes. This may give systematic errors, where particles are transported to areas with very high death rates and consequently few or none early juveniles.

The particle tracking experiments gave a large loss of particles to the north, east of Svalbard. This was linked to particular weather events in March-April. It is likely that this might happen in nature as well, but it can not be detected from the 0-group data. The reason is partly because the 0-group surveys do not cover the northernmost part of the area and perhaps also poor survival conditions in this area.

The remaining particles were transported towards south and west, partly on and partly north of Svalbardbanken. The measurements found medium to high concentrations of early juvenile polar cod in this area. The model results are therefore consistent with the hypothesis that these early juveniles were spawned in the area south-east of Edgeøya.

The measurements also have high concentration of early juvenile polar cod west of Spitzbergen each year. The model was not able to reproduce this part of the distribution. The model results seem to be consistent with a hypothesis on local spawning west of Spitzbergen. The model domain was not constructed to test such a hypothesis, and the area is very close to the boundary where the model results are most uncertain. More probably, this is a failure in the model. Such a failure may be caused by the weakness of the flow of Arctic Water from north-east in the model,

resulting in too weak current towards north on the narrow shelf west of Spitzbergen.

Another possible spawning area is Storfjorden. Westerly and northerly wind conditions, like in June 1988, may easily force the larvae southwards and onto Svalbardbanken. The 0-group surveys do not cover Storfjorden. The surveys results, however, often show decreasing concentrations towards Storfjorden. Therefore it is not likely that the main spawning areas of polar cod will be found in Storfjorden. The inner part of Storfjorden is not covered by the 4 km model, and some of the particles are lost at this boundary. This indicate that early juveniles in the Storfjorden area can be imported from the open sea.

From the above, the model results give no reason to doubt the hypothesis on spawning south-east of Edgeøya. The sensitivity studies showed that the model distributions were not very sensitive to the precise spawning time and location. As minor modifications of the initial state gave more or less the same distribution of particles, it is not possible to infer the spawning area and time of polar cod with high precision from these model results.

BIBLIOGRAPHY

ÅDLANDSVIK, B. 1989. *Wind-driven variations in the Atlantic inflow to the Barents Sea.* ICES C.M. 1989 / C:18.

ÅDLANDSVIK, B. 1997. *Sensitivity Studies of a Lagrangian Particle Transport Model.* Institute of Marine Research (in preparation).

ÅDLANDSVIK, B., & LOENG, H. 1991. A Study of the Barents Sea Climate System. *Polar Research*, **10**, 45–49.

ÅDLANDSVIK, B., & SUNDBY, S. 1994. Modelling the Transport of Cod Larvae from the Lofoten Area. *ICES mar. Sci. Symp.*, **198**, 379–392.

BARTSCH, J., & KNUST, R. 1993. *Simulating the dispersion of vertically migrating sprat larvae* (Sprattus sprattus *L.) in the German Bight with a circulation model system.* Submitted to Fisheries Oceanography.

BARTSCH, J., BRANDER, K., HEATH, M., MUNK, P., RICHARDSON, K., & SVENDSEN, E. 1989. Modelling the advection of herring larvae in the North Sea. *Nature*, **340**, 632–636.

BERNTSEN, J., SKAGEN, D.W., & SVENDSEN, E. 1994. Modelling the transport of particles in the North Sea with reference to sandeel larvae. *Fish. Oceanogr.*, **3**, 81–91.

BLUMBERG, A.F., & MELLOR, G.L. 1987. A description of a three-dimensional coastal ocean circulation model. *In:* HEAPS, N. (ed), *Three-Dimensional Coastal Ocean Models.* Coastal and Estuarine Sciences, vol. 4. American Geophysical Union.

DAMM, P. 1989. *Klimatologischer Atlas des Salzgehaltes, der Temperatur und der Dichte in der Nordsee, 1968–1985.* Tech. rept. 6–89. Institut für Meereskunde der Universität Hamburg.

EIDE, L.I., REISTAD, M., & GUDDAL, J. 1985. *Database av beregnede vind og bølgeparametre for Nordsjøen, Norskehavet og Barentshavet, hver 6. time for årene 1955–81.* Tech. rept. The Norwegian Meteorological Institute.

ENGEDAHL, H. 1995. Use of the flow relaxation scheme in a three-dimensional broclinic ocean model with realistic topography. *Tellus*, **47A**, 365–382.

ENGEDAHL, H., ÅDLANDSVIK, B., & MARTINSEN, E.A. 1995. *Production of monthly mean climatological archives of salinity, temperature, current and sea level for the Nordic Seas.* Research Report No. 3, The Norwegian Meteorological Institute.

GJEVIK, B., NØST, E., & STRAUME, T. 1990. *Atlas of tides on the shelves of the Norwegian and the Barents Seas.* Statoil report F&U-ST 90012.

GJEVIK, B., NØST, E., & STRAUME, T. 1994. Model simulations of the tides in the Barents Sea. *J. Geophys. Res.*, **99**, 3337–3350.

GJØSÆTER, H., & ANTHONYPILLAI, V. 1995. *Utbredelse av polartorsk i Barentshavet.* Fisken og Havet 23–1995, Institute of Marine Research.

HARMS, I. 1992. A numerical study of the barotropic circulation in the Barents and Kara Seas. *Cont. Shelf Res.*, **12**, 1043–1058.

HARMS, I.H. 1994. *Numerische Modellstudie zur winterlichen Wassermassenformation in der Barentsee.* Ph.D. thesis, Zentrum für Meeres- und Klimaforschung der Universität Hamburg.

JOHANSEN, Ø., MATHISEN, J.P., & STEINBAKKE, P. 1988. *Environmental data collection in the Barents Sea.* Tech. rept. OCE88059. OCEANOR.

KOWALIK, Z., & PROSHUTINSKY, A.YU. 1995. Topographic enhancement of tidal motion in the western Barents Sea. *J. Geophys. Res.*, **100**(C2), 2613–2637.

LEVITUS, S. 1982. *Climatological atlas of the world ocean.* NOAA Prof. Pap., 13.

LI, S. 1995. *The Dynamics of a Slope Current in the Barents Sea.* Ph.D. thesis, The Norwegian Institute of Technology. NTH 1995:109.

LOENG, H. 1986. *Ecological investigations in the Barents Sea, August 1985. Report from PRO MARE-cruise no.5.* Havforskningsinstituttet, Rapport nr.FO 8605.

LOENG, H. 1991. Features of the physical oceanographic conditions of the Barents Sea. *Polar Research*, **10**, 5–18.

LOENG, H., & HANSEN, S.E. 1997. *Current measurements in the Barents Sea in the period 1972–1994, an overview.* Fisken og havet, Institute of Marine Research.

LOENG, H., OZHIGIN, V., & ÅDLANDSVIK, B. 1995. *Water fluxes through the Barents Sea.* ICES J. mar. Sci. in press 1997.

MARTINSEN, E.A., & ENGEDAHL, H. 1987. Implementation and Testing of a Lateral Boundary Scheme as an Open Boundary Condition in a Barotropic Ocean Model. *Coastal Engineering*, **11**, 603–627.

MCCLIMANS, T.A., & NILSEN, J.H. 1993. Laboratory simulation of the ocean currents in the Barents Sea. *Dynamics of Athmospheres and Oceans*, **19**, 3–25.

MELLOR, G. L., & YAMADA, T. 1982. Development of a Turbulence Closure Model for Geophysical Fluid Problems. *Rev. Geophys. Space Phys.*, **20**, 851–875.

MELLOR, G.L. 1995. *User's guide for a three-dimensional, primitive equation, numerical ocean model.* Atmospheric and Oceanic Sciences Program, Princeton University.

PARSONS, A.R. 1995. *On the Barents Sea Polar Front in Summer and Interpretations of the Associated Regional Oceanography using an Arctic Ocean General Circulation Model.* Ph.D. thesis, Naval Postgraduate School.

SAMEOTO, D. 1984. *Review of Current Information on Arctic Cod (Boreogadus saida Lepechin) and Bibliography.* Bedford Institute of Oceanography. 71 pages.

SLAGSTAD, D., & STOKKE, S. 1994. *Simulering av strømfelt, hydrografi, isdekke og primærproduksjon i det Nordlige Barentshav.* Fisken og Havet, 9: 1994, Institute of Marine Research.

SLAGSTAD, D., & STØLE-HANSEN, K. 1991. Dynamics of plankton growth in the Barents Sea: model studies. *Polar Res.*, **10**, 173–186.

SLAGSTAD, D., STØLE-HANSEN, K., & LOENG, H. 1990. Density driven currents in the Barents Sea calculated by a numerical model. *Modeling, Identification and Control*, **11**, 181–190.

STØLE-HANSEN, K., & SLAGSTAD, D. 1991. Simulation of currents, ice melting, and vertical mixing in the Barents Sea using a 3-D baroclinic model. *Polar Res.*, **10**, 33–44.

SVENDSEN, E., FOSSUM, P., SKOGEN, M.D., ERIKSRØD, G., BJØRKE, H., NEDREAAS, K., & JOHANNESEN, A. 1995. *Variability of the drift patterns of Spring Spawned herring larvae and the transport of water along the Norwegian shelf.* ICES C.M. 1995/Q:25.

WERNER, F.E., PAGE, F.H., LYNCH, D.R., LODER, J.W., LOUGH, R.G., PERRY, R.I., GREENBERG, D.A., & SINCLAIR, M.M. 1993. Influences of mean advection and simple behavior on the distribution of cod and haddock early life stages on Georges Bank. *Fish. Oceanogr.*, **2**, 43–64.